Paleotopographic control of landslides in lacustrine deposits (Trièves plateau, French western Alps)

Grégory Bièvre, U. Kniess, Denis Jongmans, E. Pathier, S. Schwartz, Thierry Villemin, Cees van Westen, Vilma Zumbo

Combined use of remote-sensing and ground geophysical techniques to investigate geological control on landslides (Trièves area, Western Alps, France)

Grégory Bièvre[a,b], Ulrich Knieß[a], Denis Jongmans[a,*], Erwan Pathier[a], Stéphane Schwartz[a], Thierry Villemin[c], Cees J. van Westen[d], Vilma Zumbo[b,e]

[a] *Laboratoire de Géophysique Interne et Tectonophysique, CNRS, Université Joseph Fourier, BP 53, 38041 Grenoble cedex, France*
[b] *Centre d'Études Techniques de l'Équipement de Lyon, Laboratoire Régional d'Autun, BP 141, 71405 Autun cedex, France*
[c] *Laboratoire Environnements Dynamiques et Territoires de Montagne, CNRS, Université de Savoie, 73376 Le Bourget-du-Lac, France*
[d] *International Institute for Geo-Information Science and Earth Observation (ITC), Hengelosestraat 99, 7500 AA, Enschede, The Netherlands*
[e] *Inexia-Ingénierie, Département Infrastructures et Amńagement, 1 Place aux Étoiles, 93212 Saint-Denis-La-Plaine Cedex, France*

Abstract

This paper presents a study combining remote sensing and seismic prospecting for investigating two clayey landslides located in the Trièves area (Western French Alps). Although affecting similar slopes made of similar clay layer under the same meteorological conditions, the two adjacent Avignonet and Harmalière landslides exhibit, since the 1980s, major differences in morphology, displacement rate magnitudes and motion directions. These observations suggest the control of at least one additional internal factor on the landslide characteristics. Combination of geological mapping, airborne Light Detection and Ranging (LiDAR) data, aerial photographs, Global Positioning System (GPS) and seismic noise measurements allows characterizing the landslide

*Corresponding author.
Email addresses: gbievre@ujf-grenoble.fr (Grégory Bièvre), ukniess@ujf-grenoble.fr (Ulrich Knieß), djongmans@ujf-grenoble.fr (Denis Jongmans), epathier@ujf-grenoble.fr (Erwan Pathier), sschwartz@ujf-grenoble.fr (Stéphane Schwartz), thierry.villemin@univ-savoie.fr (Thierry Villemin), westen@itc.nl (Cees J. van Westen), vilma.zumbo@inexia-ingenierie.com (Vilma Zumbo)

morphology and the thickness of the soft layer down to the seismic substratum, providing a 3D view of the soft layer bottom. GPS measurements and digital photographs reveal that the difference in kinematics between the two earthslides can be tracked back to 60 years ago at least. The Avignonet slide is mainly directed towards the East while Harmalière is mainly oriented towards SE. The LiDAR scan map illustrates this differential motion and morphology between the two slides and highlights that the Harmalière slide is still presently much more active than the Avignonet one. A ground geophysical prospecting based on ambient noise measurements allowed to map the base of the clays and indicates the presence of a N-S ridge of hard sediments (Jurassic bedrock and/or compact alluvial layers) on the eastern side of the Avignonet landslide. This ridge disappears when approaching the Harmalière landslide and makes place to what can be interpreted like a NW-SE oriented palaeovalley of the river Drac. It is proposed that the ridge could act as a butress which could mechanically prevent the Avignonet landslide from evolving as fast as the Harmalière one. Furthermore the NW-SE palaeovalley located under the Harmalière landslide corresponds to the motion direction of the slide. It is then finally proposed that the slides different behaviours are partly controlled by the palaeotopographic setting of lake Trièves. These results suggest a major influence of the bedrock palaeotopography on the kinematics of the two landslides.

Keywords: Clay landslides, LiDAR, GPS, aerial photographs, microtremors, differential kinematics, palaeotographic control

1. Introduction

. This paper presents a study combining remote sensing and seismic prospecting for investigating two clayey landslides (Avignonet and Harmalière) located in the Trièves area (Western Alps; Fig. 1). Although affecting similar slopes made of similar clay layer under the same meteorological conditions, these two adjacent landslides exhibit, since the 1980s, major differences in morphology, displacement rate magnitudes and motion directions. These observations suggest the control of at least one additional internal factor on the landslide characteristics. Such control by lithological variations, hydrogeological drainage or structural features have been regularly depicted in clay slides (Bonci et al., 2004; Lapenna et al., 2005; Eilertsen et al., 2008; Bozzano et al., 2008). This study aims to explain the significant differences in geometry and kinematics observed between the landslides of Avignonet and Harmalière. Combination of geological mapping, airborne Light Detection and Ranging (LiDAR) data, aerial photographs, Global Positioning System (GPS) and seismic noise measurements allows characterizing the landslide morphology and the thickness of the soft layer down to the seismic substratum, providing a 3D view of the soft layer bottom. This reveals the palaeotopography upon which settled the clays and helps to assess the geological control on the two landslides behaviour.

. In the last two decades, remote sensing techniques and geophysical prospecting methods have been increasingly used to image landslide structures at the surface and at depth, respectively. Remote sensing techniques, such as radar interferometry, high-resolution optical images correlation and multi-temporal laser scanning, allow the surface displacement field to be measured, which

is a key parameter to understand the landslide mechanics (for a review, see Metternicht et al., 2005; Delacourt et al., 2007). In complement to conventional ground-based geodetic techniques and GPS surveys that provide only a limited number of discrete measurements, multi-temporal remote sensing imagery has the potential to measure nearly continuous displacement rate field over landslides (among others, Fruneau et al., 1996; Rott et al., 1999; Kimura and Yamaguchi, 2000; Squarzoni et al., 2003; Metternicht et al., 2005; Strozzi et al., 2005; Corsini et al., 2007). Nonetheless, performances of the remote sensing techniques strongly depend on the site conditions (slope steepness and orientation, vegetation, size, slide velocity) and on weather conditions. These techniques that can be borne on various platforms (space, aerial or ground) and combined together, can achieve decimetric to centimetric resolution and accuracy in favorable conditions (Delacourt et al., 2007). In the last few years, both airborne and ground LiDAR techniques have been increasingly applied for mass movement studies, particularly in steep and rugged terrain (e.g. Thoma et al., 2005; Abellan et al., 2006; Corsini et al., 2007; Deparis et al., 2008; Oppikofer et al., 2008). Recently, airborne LiDAR images were successfully used to map recent and historical landslides in gentle slope areas (Schulz, 2007; Van den Eeckhaut et al., 2007). Major advantages of LiDAR technique are the flexibility and the quickness of the acquisition as well as the relatively simple data processing, allowing multi-temporal Digital Elevation Models (DEMs) to be generated (McKean and Roering, 2004; Rosser et al., 2005; Thoma et al., 2005; Oppikofer et al., 2008).

In parallel, shallow geophysics has also considerably evolved with the emergence of 2D and 3D spatial imaging, allowing the study of the spatial

and temporal variations inside landslides (for a recent review, see Jongmans and Garambois, 2007). Geophysical imaging has the major advantages to give continuous information on the studied body and to be non-invasive. However, resolution generally decreases with depth. Geophysical prospecting applied to landslides encompasses a large number of techniques: seismic reflection, seismic refraction, electrical resistivity tomography (ERT), seismic noise measurements, spontaneous potentials, electromagnetic, Ground Penetrating Radar (GPR) and gravimetry. Flexible and quick to deploy, these techniques have been applied on various types of landslides for slope varying from a few degrees (earth slide) to vertical (rock fall), with a penetration depth of the surveys ranging from 3 m to 400 m (Green et al., 2007; Heincke et al., 2006; Jongmans and Garambois, 2007).

. Although remote sensing and geophysical techniques are complementary for landslide imaging purposes, they have been rarely associated. Roch et al. (2006) and Deparis et al. (2008) combined remote and ground imaging techniques for determining the geometry and the 3D fracture pattern of potentially unstable cliff sites. A dense digital surface model of the rock face was measured from laser scanning (LiDAR) and/or photogrammetry, while the GPR performed on the cliff allowed the discontinuity pattern inside rock mass to be obtained. On low slope made of clay-rich sediments, Perrone et al. (2006) presented a joint analysis of SAR interferometry and ERT surveys for investigating and understanding complex ground deformation of different origin. Brückl et al. (2006) utilized photogrammetric, GPS and seismic data to derive the kinematics of the Gradenbach deep-seated landslide (Austria) affecting crystalline rocks.

. In the following, the geological setting of the study area is first assessed. Then, the use of LiDAR data, aerial photos and GPS measurements will lead to better constrain the two landslides activity and extent as well as their kinematics. The easy-to-deploy and fast H/V prospecting will allow to estimate the soft layer thickness. The original combination and integration of these techniques will help to build a 3D view of the soft layer and assess a possible geological control on the landslides.

2. Geological structure and mapping

. The Trièves area is located 40 km south of the city of Grenoble in the external French Alps (Fig. 1). This plateau region with a maximum altitude of 800 m above sea level (asl) corresponds to a large depression of about 300 km^2 drained by the Drac river and its tributaries. It is bordered, to the West and to the South by the Vercors and Dévoluy carbonate massifs, respectively. To the East, it is limited by the southern end of the crystalline Belledonne range (Fig. 1). This area is the main outcrop of quaternary glaciolacustrine clays. Many landslides affect this zone among which 15 % are supposed to be sliding (Lorier and Desvarreux, 2004). These slides might affect surfaces as large as 1 km^2. They can develop over several slip surfaces ranging from superficial (5 m to 15 m) to rather deep (down to 50 m; Blanchet, 1988; Jongmans et al., 2009). Slide velocities are generally low (a few cm/year) but can reach several m/year in certain places. In some cases, generally after a long wet period accompanied by quick snowmelt, the slides can evolve into a mudflow and velocities can reach several m/h. This lead to dramatic events in Harmalière in 1981 (Moulin and Robert, 2004) and in La-Salle-en-Beaumont

in 1994 (Moulin and Chapeau, 2004). This important gravitational instability is mainly related to the Quaternary geological history of the region. It was controlled by several glacier fluctuations, which resulted in alternating deposition and erosion phases. The particular geometrical setting and the sediments recorded these major climatic fluctuations.

. The substratum on which rely the quaternary formations is made of early Jurassic carbonate strata which were folded and faulted during the alpine orogenesis. Ancient glacial (Riss) and interglacial phases (Riss-Würm) carved the substratum and generated valleys partly filled with Riss-Würm alluvial deposits. This lead to an irregular shape of the basement prior to the last glacial phase (Würm; -80 to -12ky BP). During the last glacial maximum extension (LGM, Würm period, -22 to -18 ky BP; Clark et al., 2009), the Isère glacier, coming from the North, blocked downstream the torrential flows from the Drac river and its tributaries, generating an ice-dammed lake (lake Trièves, Fig. 1; Monjuvent, 1973). This lake was progressively filled during thousands of years mainly by millimetric to decimetric rythmic alternations of clay and silt layers originating from nearby Mesozoic marls and crystalline massifs (Huff, 1974). These laminated clays rest either on carbonate or alluvial, locally cemented, compact layers from the interglacial Riss-Würm period. The irregular shape of the basement induces strong lateral thickness variations of the palaeolake infill, from 0 to more than 250 m (see Figs. 2 and 3; Monjuvent, 1973; Antoine et al., 1981). The top of the clay is generally found at an elevation of about 750 m asl (Antoine et al., 1981). Morainic deposits which cap the clays are found as far as the south of the village of Sinard, indicating the southward limit of the würmian glacier extension

(Figs. 1 and 2). Also, these moraines are not present in the downslope parts of landslides, where clays outcrop (Fig. 2). At the study site, their thickness evolves, around Sinard, from 50 m to the West to a few meters to the East. At the end of the LGM in Europe, the Isère glacier withdrew, allowing the rivers to cut deeply into the formations. This last erosion phase created the actual Drac river valley. This favoured the conditions for landslide development in the clay with a general Eastward motion in the study area (Fig. 2; Brocard et al., 2003; Jongmans et al., 2009).

. The geological map and the cross-section of figures 2 and 3, respectively, show the geometrical arrangement of the geological formations in presence. Two palaeovalleys, labelled v1 and v2 on figure 3, depict previous interglacial incision phases. Palaeovalley v1 is the oldest one (Monjuvent, 1973; Brocard et al., 2003). Both palaeovalleys are filled with locally cemented alluvial layers. They have been recognized by field observations and, under the clay cover, by geophysical investigations conducted in the 1950s for the construction of the Monteynard dam (location in Fig. 2; Crosnier-Leconte et al., 1953; Monjuvent, 1973). In the study area (Fig. 1), these erosion and deposition phases resulted in an irregularly shaped substratum top (Fig. 3). The last erosion phase, at the end of the LGM, resulted in the actual Drac river valley. A general view from the opposite side of the lake is presented on figure 4a. Jurassic bedrock, quaternary alluvial layers and laminated clays are shown on outcroup pictures of figures 4b, 4c and 4d, respectively.

3. Landslide geomorphology and history

3.1. Techniques

In this part we will focus on the comparison between the Avignonet and Harmalière landslides. Three techniques have been used to analyze and compare the geomorphology and kinematics differences of these slides. To obtain a DEM for geomorphological interpretation a LiDAR laser scan, covering the two landslides, was performed. Aerial photographs and GPS measurements were used to analyse the kinematics back to 1948.

. The LiDAR scan was performed in November 2006 using the handheld airborne mapping system Helimap® (Vallet and Skaloud, 2004) mounted on a helicopter flying about 300 m above the terrain. The landscape is characterized by forest, agriculture and grassland. There are no artificial structures on Harmalière but a few small roads, 3 piles of an electric landline and 54 buildings on the Avignonet landslide. The time for the acquisition was chosen to be in November, so that the leaf coverage has already decreased and snowfall has not started yet. The system has recorded 36 million last pulses of the surface reflection resulting in an average of 6 points per m^2 with an accuracy of 10 cm in vertical and horizontal directions. In order to derive the bare earth model excluding trees and houses the point cloud was filtered and interpolated to a 2 m raster grid with the software SCOP++® IPF (2004) using the *robust interpolation* method (Briese et al., 2002). The number of points classified as ground reflections and therefore used for the griding of the DEM is 21 million, which is equivalent to an average of 3 points per m^2. The resulting shaded DEM is shown in figure 5. Shaded representations with

different light angles were used for geomorphologic interpretation.

. GPS campaign measurements have been performed biannually (April and November) since 1995 by RTM (*Restauration des Terrains en Montagne*, a french public survey) at 25 points on the Avignonet landslide (Fig. 5), relatively to several reference points located on nearby stable bed-rock. The average standard deviation for all measured points is 6 mm. No GPS measurements have been done so far inside the Harmalière landslide, because of the quick surface evolution making benchmark installation difficult. Average horizontal velocity vectors are shown in figure 5. No clear temporal pattern of velocity changes emerges from the data certainly due to the low temporal sampling.

. To analyze the kinematics further in the past, digital photogrammetric scans of aerial photographs from IGN (*Institut Géographique National, France*) of the years 1948, 1956, 1978, 1985, 1993, 2001 and 2003 at scales between 1:20 000 and 1:30 000 covering the two landslides have been used. The photos were orthorectified with the software Geomatica® using the DEM BD-ALTI® from IGN with a resolution of 50 m (the LiDAR DEM was not covering a large enough area to be used), the calibration certificates of the utilized cameras and 56 ground control points measured on the field with differential GPS. The ortho-photos have been analyzed to investigate the landslide activity through time. The mapping of the denuded area and of the headscarps was found to be useful indicators of landslide activity.

In the studied area, bare soil (mostly clays) can be observed in several places, over significantly large surface (from about 250 m^2 to more than 50000 m^2 in Harmalière). Where field observation has been done, it turns out

that these bare soil surfaces result from erosion and weathering processes in relation to superficial landslide activities. In the following the term denuded area is used to refer to these surfaces. To quantify the spatial and temporal distribution of denuded area over the whole studied area, aerial photos have been used.

When comparing field observations at Harmalière and Avignonet landslides with ortho-photos, denuded area appears as very bright pixels in aerial photography compared to the surrounding forested or agricultural landscape except for some field crops, the river and some human constructions (road, buildings) that can also be bright (see Fig. 6, top). Consequently, for each ortho-photo, pixels have been classified as denuded area, using as reference the level of brightness of areas where bare soil has been observed in the field, and excluding the river (or the lac), bright fields, roads and buildings identifiable by their characteristic geometric shapes (see Fig. 6, bottom).

3.2. Analysis

Using the three sets of data, as described in the previous section, several features can be analyzed to highlight the difference in kinematics between the Avignonet and Harmalière landslides: the general orientation of the landslide, surface velocity, denuded area, headscarp evolution and surface roughness.

. The clay area affected by sliding is larger on Avignonet (1.8 km^2) than on Harmalière (1.2 km^2). The headscarps of Harmalière and Avignonet mapped from the 1956 aerial photo (before the construction of the Monteynard Dam), show that the maximum distance between the headscarps and the Drac Valley is about 1.5 km in both cases. Both headscarps follow a curve that have a

symetry axis oriented NNW-SSE, perpendicular to the Drac Valley, as it is expected in a homogeneous clay mass deeply cutted by a valley (see Fig. 6 on the bottom left). In Avignonet, the global sliding direction follows this axis as expressed by the fan-shape pattern of the GPS velocity vectors and of the slope directions of the main scarps. The 11-years average velocity vectors from GPS on the Avignonet landslide are oriented from N 70 ° E to N 130 ° E (Fig. 5), with a global N 100 ° E movement.

However, in Harmalière, according to the evolution of denuded area, the most active areas of the landslide develop along a NNW-SSE axis (Fig. 6) making a 30 ° angle with the Avignonet global sliding direction. The percentage of denuded surface is much larger in Harmalière than in Avignonet since the first photos in 1948 (13 % versus 5 % in 1948, 20 % versus 3 % in 1984 and 19 % versus 3 % in 2003). Only a very small active area in the south of Avignonet can be identified. The higher activity of Harmalière certainly goes back, at least, to the end of the 19th century: at that time, according to Moulin and Robert (2004), because of intense gully erosion occurring on the NW part of the Harmalière slide, a significant reforestation work has been implemented by the state authorities. Since the catastrophic Harmalière event in 1981, denuded area are more concentrated in the eastern part of the Harmalière landslide and has grown up-slope since then. Morphological changes due to the 1981 event can be seen in the 1985 sketch of figure 6 forming a NNW-SSE elongated body of denuded areas and also in figure 5 where, at the same place, a roughness contrast with the surroundin terrain can be noticed. The body itself can be divided into a steeper upstream part where erosion dominates and a smoother lower part corresponding to an accumu-

lation zone, which has been conquered by trees again since the 1981 event (Fig. 6 on the right). It is noteworthy that the recent up-slope evolution is not directed straight to the NW, but has rotated clockwise to the N-NE toward the Avignonet landslide.

The main headscarp of Harmalière, which has developed since the catastrophic event of March 1981, has mainly regressed through several brutal events (biggest events were in 1988, 1996 and 2001; Moulin and Robert, 2004). This evolution is traceable from aerial photos analysis, providing a mean regression rate of about 10 m/year between 1981 and 2003. These values are in agreement with ground observations (Moulin and Robert, 2004). Since 2001, the headscarp regression has started to affect the southern limit of the Avignonet landslide. A GPS measurement on the crest between Harmalière and Avignonet indicates mass displacement towards the Southwest, which is consistent with a faster regression of the Harmalière scarp toward the Northeast (Fig. 6) relative to Avignonet. To the North of Harmalière the limits with another landslide show a convexity toward the south (Fig. 5 and 6). On the LiDAR DEM, in the northern part of Avignonet slide, the four uppermost major scarps (spaced by about one hundred of meter) seems to be cut by the northern limit. This suggests that the northern landslide has been the last to be the most active with respect to the Avignonet one.

. Surface roughness is also an indicator for landslide activity (Glenn et al., 2006). Analysis of surface roughness from the shaded LiDAR DEM (Fig. 5) shows differences between the Harmalière and Avignonet landslides in terms of wavelengths and amplitudes along the slope direction. In Harmalière, a characteristic small-scale roughness with wavelengths of 5-15 m and ampli-

tudes of 0.5-5 m can be observed, as well as roughness at a larger scale with wavelengths of 80-200 m and amplitudes of 5-20 m. Two representative elevation profiles along the slope direction are shown in Fig. 5b. They are divided into an upper and a lower part according to the presence of significant changes of slope angle and roughness. On these profiles, the roughness has been estimated using the root-mean-square deviations as described by Shepard et al. (2001) with step-sizes of 10 m and 100 m along with the mean slope angles (see table 1) corresponding small-scale roughness and large-scale roughness at the wavelengths of 10 m and 100 m respectively. In Avignonet the roughness is higher at the toe (1.6 m) than in the upper part (1.1 m) for the small-scale roughness, which can be explained by the higher activity down-slope, as suggested by the GPS, associated to a higher slope angle and may be a higher erosion rate. In Harmalière, the roughness is lower in the lower part than in the upper part for both wavelengths. Indeed, since 1981, Harmalière has shown intense activity in its upper part including collapsing at the headscarp and several minor scarps below, that are responsible in a higher large-scale roughness (5.4 m). In the lower part, it evolves into a more fluent mudslide (large-scale roughness at 2 m) related to the development of an accumulation zone which presents a lower slope angle. Similar large-scale roughness values are found for the upper parts of Avignonet and Harmalière. Assuming that features related to large-scale roughness are more robust through time that the small-scale one, this observation suggests that Avignonet and Harmalière have experienced similar landslide processes in the past. It must be stated that using roughness as an indicator of landslide activity can be biased by several factors that should be discussed. First

of all the density of data points after filtering when building the DEM can influences the roughness. Data density decreased in forested area because of the filtering and could lead into lower roughness. In figure 5, the constructed DEM is resampled at 2 m resolution: beside a few exceptions and after filtering the forest, the laser points were still dense enough to avoid smoothing effects due to interpolation. For instance, the south-western part of the Harmalière landslide, which is largely forested, show a higher small-scale roughness than the farming area of the Avignonet slide. On the other hand the effect of farming altering the surface roughness should also be considered. On a very small scale farming can decrease the surface roughness in a very short time, but also high scale roughness could be decreased by farming over decades. On the other hand if the activity of the landslide and with that the roughness is too high, the field will become abandoned and the roughness will be not further decreased. Therefore it can be said that farming amplifies the trend: smooth areas will be more smoothed and rough areas will stay rough above a certain threshold. If there are other causes to abandon a field then the landslide activity, the interpretation of roughness can be misleading. In the case of Harmalière, it can be observed from the aerial photos that a lot of fields become abandoned after being affected by the past 1981 events. Today farming is completely stopped on Harmalière. Also the active part in the south of Avignonet was partly farmland in the past and become abandoned recently.

Taking into account these limitations, the roughness comparison between the Avignonet and Harmalière slide still suggests a significant difference of the recent sliding activity: the Avignonet slide do not show major recent active

movements in agreement with GPS data and aerial photographs analysis, in contrast to the Harmalière slide. Only some areas in the lower part and in the South of Avignonet exhibit small-scale roughness similar to Harmalière. This is consistent with the location of denuded area in the most recent aerial photos, which are correlated to a higher landslide activity.

. Regarding slide velocity, values measured by GPS at the surface of the Avignonet landslide (Fig. 5) increase from less than 20 mm/year at the top to more than 130 mm/year in the most active parts at the toe. The aerial photos show no major signs of activity in Avignonet for the last 60 years with no significant evolution of the headscarp and very small denuded areas. In Harmalière no GPS measurements are available but, by tracking morphological features through different dates in the aerial photos, one can get a rough estimate of the average velocity of several meters per year for some parts of the main landslide body, which is significantly higher than in Avignonet.

. Comparison of the two landslides by LiDAR scan, GPS data and aerial photos has shown that the recent and former landslide kinematics are highly different for the two earth slides. Harmalière seems to be much more active than Avignonet, today and in the past 60 years. A major factor for this could be the underlying bedrock topography. This possible influence parameter is investigated in the following section.

4. Geophysical investigation

. The objective of the geophysical investigation is to map the thickness of the soft layer over the two landslides. This thickness ranges from 0 to more

than 250 m from the East to the West, respectively (Antoine et al., 1981). The site to be characterized encompasses a surface of 5 km^2. Geological investigations conducted in the 1950s for the study of the Monteynard dam (location in Fig. 2) were limited to the Avignonet area. No information is available about the geological setting of the Harmalière area. Furthermore, geophysical campaigns which aimed to characterize the geological setting in the immediate vicinity of the dam were not published and only synthetic data are available. This poses the problem of the reliability of the established model of figure 3.

Recent works (Jongmans et al., 2009) have shown the existence of a strong shear wave (S-wave) velocity contrast (more than 3 on average) between the soft upper layers (clays and moraines; 250 m/s $<$ Vs $<$ 600 m/s) and the substratum made of compact cemented alluvial layers (Vs = 1250 m/s) and Jurassic limestone (Vs = 2000 m/s). With such characteristics, microtremor processing (H/V technique) has been proven to be one of the most robust and easy exploration tool for mapping the thickness of alluvial or lacustrine sediments (Ibs-von Seht and Wohlenberg, 1999; Delgado et al., 2000; Guéguen et al., 2007; Méric et al., 2007; Le Roux et al., 2008) including the Trièves area (Jongmans et al., 2009).

4.1. Method

The H/V technique is a single station method consisting in calculating the horizontal to vertical spectral ratios (H/V) of seismic noise records. For a single homogeneous soft horizontal layer (1D geometry) overlying the bedrock, the H/V curve exhibits a peak at a frequency f_{HV} that is the shear-wave resonance frequency f_0 of the soft layer (Bard, 1998). This theoretical resonance

frequency is given by (Haskell, 1960):

$$f_0 = \frac{V_s}{4T} \tag{1}$$

where Vs is the soft layer S-wave velocity (in m/s) and T is the layer thickness (in m). The resonance frequency decreases with a decrease of Vs and an increase of thickness. If Vs is known, this equation allows the layer thickness to be determined. For a layered medium overlying a halfspace, the resonance frequency can be computed from the thickness and the dynamic characteristics of each soil layer (Haskell, 1960) and the total thickness of the soil layers can be deduced if the vertical velocity profile is known. When the seismic impedance contrast Z between the soft layer and the bedrock is high enough (Z > 4), the H/V peak was shown to result from a change in the ellipticity of the fundamental mode of the Rayleigh waves (Bonnefoy-Claudet et al., 2006). The corresponding ellipticity frequency f_{ell} is then equal to the resonance frequency f_0.

Measurements were made with a single three-component 5 s sensor giving a flat response between 0.2 and 50 Hz and connected to a light seismic acquisition system (Chatelain et al., 2000). Seismic noise was recorded during 15 minutes with a 200 Hz sampling frequency. Data were processed with the Sesarray package (wwww.geopsy.org; Wathelet et al., 2004). Microtremor records were cut into 30 s time windows, for which Fourier spectra were computed and smoothed using the technique proposed by Konno and Ohmachi (1998). H/V spectral ratios were computed for all time windows and the mean H/V curve is given with standard deviations at each site.

The H/V method offers the advantages of being easy to deploy (one

station-one people) and quick (about 10 sites per day), depending on field conditions. Limits are weather conditions, likely to influence the H/V curve (Koller et al., 2004), and the assumption of horizontally layered medium, which cannot be valid in case of strong lateral seismic contrasts (Uebayashi, 2003). In the study site conditions, the 5 km^2 area was covered within a two weeks delay by a single operator.

4.2. H/V data

H/V measurements were performed at 104 sites (Fig. 7) and were located with a GPS with a horizontal accuracy ranging from one to a few meters under forest. Elevation values were extracted from the LiDAR DEM. H/V curves (spectral ratio versus frequency) at two sites (S1 and S2) are presented in figure 7a. Both curves exhibit a peak with amplitude over 8 at 0.58 Hz for S1 and at a 3.63 Hz for S2, corresponding to the resonance frequency of the site. At S2, a second peak appears at 20 Hz, which could correspond to the resonance of a superficial layer or to a higher resonance mode. The great majority of the 104 measured H/V curves fit the criteria proposed in the SESAME guideline (Koller et al., 2004) for a 1D resonance phenomenon, with well-individualized peaks and H/V amplitudes greater than 2. For some measurements, located in the southeastern part of the Harmalière landslide (location in Fig. 7b), however, curves exhibit a plateau-like shape, suggesting 2D or 3D effects. This point will be discussed below.

. The frequency field was gridded with a kriging algorithm (Kitanidis, 1997), using an exponential variogram model with a N-S anisotropy for the search radius. The gridded surface fits the experimental data with an absolute error

of 3 %. The results are presented on figure 7c.

. To the West, the frequency map (Fig. 7c) reveals a NNE-SSW 500 m wide elongated low-frequency zone, with values ranging from 0.4 to 1 Hz. To the East, frequencies increase rapidly with distance, from 1 to 4 Hz. This eastward evolution of the resonance frequency is consistent with the thinning of the clay layer and the corresponding rise of stiff layers shown in previous works (Fig. 3; Crosnier-Leconte et al., 1953; Lambert and Montjuvent, 1968; Blanchet, 1988; Jongmans et al., 2009). Applying equation 1 with a mean S-wave velocity of 600 m/s in the clay layer (Méneroud et al., 1995) yields a clay thickness between 375 m to the west and 37 m to the east. These thickness values are however approximate, owing to the vertical S-wave velocity variation in the clay layer. This results from the effects of compactness and landslide activity. The dynamic characteristics (P-wave and S-wave velocities, density) within the different layers (from top to bottom: morainic colluvium, moraine, disturbed clays, undisturbed clays, alluvium and bedrock) were obtained from previous seismic studies (Méneroud et al., 1995; Renalier et al., 2007; Jongmans et al., 2009) and are presented in table 2. Thickness values in the layers were estimated at each station from the available geophysical and geotechnical data (Monjuvent, 1973; Antoine et al., 1981; Blanchet, 1988; Lorier and Desvarreux, 2004; Jongmans et al., 2009). Then, the only free parameter left is the thickness of the undisturbed clay layer.

Preliminary theoretical sensitivity tests were conducted using the Sesarray package (Wathelet et al., 2004). They have shown that the clay thickness is the main parameter controlling the resonance frequency. Furthermore, these tests also showed that the impedance contrast, using the parameters

of Table 2, between clays and cemented alluvial layers was sufficient enough to generate a peak corresponding to the resonance frequency. It implies that the measured frequency corresponds in each case to the base of the clays. No change in the f_0 value has been found when passing the landslide head-scarp (cf. Fig. 7c). Furthermore, within the slide, no high-frequency peak that could sign a shear plane has been recorded nor computed. These results support the use of resonance frequency measurements for determining the base of the clays. On an other hand, they indicate that this technique might not be suitable for detecting and mapping the slide itself (on the contrary of Méric et al., 2007). This could be due to an insufficient seismic impedance contrast between the disturbed clays and the undisturbed laminated clays (cf. Table 2).

The soft layer thickness was computed at each station by fitting the theoretical resonance frequency to the measured one using a trial and error method. The plot of computed thicknesses versus experimental resonance periods (inverse of the frequency) for the whole data set shows a good correlation (Fig. 8a), corroborating the determined velocities in the layers. The H/V deduced geometry of the seismic bedrock top is compared to the section previously established from a long refraction profile conducted for the study of the Monteynard dam (profile P1, location in Fig. 7c; Blanchet, 1988) which depicts the top of the Jurassic bedrock. A general good agreement is observed between the two sections (Fig. 8b) in terms of relative way of the palaeotopography. Observed discrepancies range from a very few m to the East to some 40 m to the West. These disparities may come from strong changes in layer velocities which are not known. This also may come from

485 the reference geological model, established from a refraction study and which
486 reliability is not known. This prevents this H/V mapping from being exhaus-
487 tive but allows the relative palaeotopography to be estimated and analyzed
488 in terms of geometry. Errors may also arise from 2D and/or 3D effects as well
489 as from varying cementation of the alluvial layers, as observed at outcrop.
490 These points will be discussed further.

491 . The thickness values obtained over the whole area were then kriged with
492 an exponential variogram model to produce a map depicting the distribution
493 of the thickness of the soft layer (moraines, morainic colluvium and clays)
494 over the seismic substratum (alluvial compact layers and Jurassic bedrock;
495 Fig. 9a). Outcrops of stiff alluvium and carbonate bedrock (0 m of soft cover
496 thickness) were added in order to better constrain the interpolation. The
497 thickness map is in agreement with the frequency map of Figure 7, showing a
498 significant westward increase of the clay thickness from 0 m on the valley flank
499 to more than 300 m below the village of Sinard. These values are consistent
500 with field observations and the outcropping of the alluvial layers to the East
501 (Fig. 3). This is also consistent with previous estimations (Monjuvent, 1973;
502 Antoine et al., 1981) that give a soft layer thickness from 0 to 300 m on the
503 West (moraines and clays; see Table 2).

504 . Thickness values were subtracted from elevation values given by the LiDAR
505 DEM at each measurement point. These points were again spatially interpo-
506 lated using a kriging method with an exponential variogram model. The relief
507 of the bottom of the clay layer is given in Figure 9b. The palaeotopography
508 upon which clays have been deposited is very irregular, with elevation varia-
509 tions of more than 150 m. The major feature is the presence of a depression

striking NNE-SSW, which is bordered to the East by a N-S ridge culminating at an elevation of about 600 to 620 m (cross-section AB on Fig. 10). This depression probably coincides with palaeovalley v2 of the palaeodrac river, as suggested by the presence of alluvial outcrops along the lake (Figs. 2 and 3) and by previous works (Crosnier-Leconte et al., 1953; Monjuvent, 1973). The N-S ridge appearing to the east and shown on cross-section AB corresponds to the presence of carbonate bedrock irregularly covered with compact alluvial layers and sporadically outcropping along the lakeshore. To the South, this ridge disappears (cross-sections AC and AD; Fig. 10). In figure 9 are superimposed the limits of the landslides of Avignonet and Harmalière. Below the southern part of the Avignonet slide, on its eastern side, the ridge of compact layers continuously extends perpendicularly to the global slide motion and could act as a buttress. On the contrary, the Harmalière landslide clearly developed over the lower elevation zone (Fig. 9b) and its motion can be explained by its orientation which changes from N-S to NW-SE in the South.

5. Discussion

. Geophysical investigation with ambient noise measurements allows to compute a frequency map (Fig. 7c) that can be turned into a soft sediments thickness map which is used to derive a paleotopography map (Fig. 9). Considering the thicknesses that have been computed, one may argue that 2D and/or 3D effects are present and that measured f_{HV} might be biased. The presence of non-1D cases is highlighted by strong lateral variations observed on the frequency map (Fig. 7a). Consequently, calibration based on the el-

lipticity of the fundamental mode of Rayleigh waves may be irrelevant and cannot provide the correct thickness for the soft layers. Some of these effects have been noticed on the signals located in the southeastern part of the Harmalière landslide (Fig. 7b) by plateau-like signals. By picking the frequency at the plateau cut-off, the resonance frequency tends to be overestimated (Guillier et al., 2006). Similar side effects have already been reported by studies conducted within small-apex valleys (Uebayashi, 2003; Koller et al., 2004; Guéguen et al., 2007; Le Roux et al., 2008). This is illustrated on cross-section AC of figure 9. Between abscissa 800 and 850 m, a bulge of substratum is visible. It corresponds to a zone with pleatau-like H/V curves. This strong side effect tends to provide an overestimated measured f_{HV} and, thus, a lowered clay thickness. As a consequence, the observed bulge on cross-section AC is likely to result from side effects and not to represent a real structure.

Another problem arising from calibrations is the eventual presence of lateral Vs variations in the soft sediments. Vertical and W-E variations are known to be present within clays (Renalier et al., 2007; Jongmans et al., 2009) and were taken into account for the frequency to thickness computations. On an other hand, since the Würm glacier extension was limited to the village of Sinard (Figs. 1 and 2), the presence of such an ice-cap and of the 50 m thick moraines may influence the compactness and, then, the S-wave velocity of the clays across this boundary. Nevertheless, N-S velocity variations within the soft layer have not been reported hitherto and were not eventually integrated to this work.

As a consequence of these uncertainties, the soft layer thickness map com-

puted from H/V data may contain more or less important error bars. These errors are estimated to a few meters to the East (were soft layer thickness is of a few tens of meters) to some 40 m to the West, were the soft layer reaches 300 m. These uncertainties do not question the reliability of the first order of observations since the aim of this work is to map the relative variations of the seismic substratum. The basement of the former Trièves lake on which were deposited the glaciolacustrine laminated clays is irregularly shaped and shows strong lateral variations. At most, this introduces an uncertainty in the exhaustive mapping of the clay thickness.

. There is a N-S ridge to the East of the investigated area, culminating at about 620 m, which disappears to the south. Cross-sections AC and AD on figure 10 illustrate the progressive vanishing of this hard ridge marking a depression to the South at about 460 m, which continues toward the North-East and then runs along the west side of the ridge. This depression allowed the deposition of 300 m of clays and moraines over a seismic substratum located at an elevation less than 520 m asl. Over the ridge only a very few tens of meters of clay remain because of a lower thickness of sediment and of erosion. This analysis confirms previous works done by other geophysical methods on Avignonet (Crosnier-Leconte et al., 1953; Blanchet, 1988), and also extents consistently the knowledge of the palaeotopography to the south up to Harmalière. The new map also confirms the geological observations and interpretation inferring that several glacial and interglacial erosion phases, that took place during the Quaternary (Monjuvent, 1973; Brocard et al., 2003), created a palaeotopography marked by the incision of at least two paleovalleys of the Drac, called "Drac de Sinard" and "Drac de Cros", filled

with alluvium and running below the laminated clay of the Sinard plateau, notably below Harmalière and Avignonet (Lambert and Montjuvent, 1968; Monjuvent, 1973). However, Lambert and Montjuvent (1968) and Monjuvent (1973) indicate that the top of the "Drac de Sinard" alluvium is at about 500-520 m asl in the Harmalière-Avignonet area, and that its bottom is at about 410 m asl, whereas our results show, west to the ridge, intermediate values ranging between 440 and 500 m asl. This could suggest that the method used is not sensible to the contrast between alluvial deposits and clay. Preliminary theoretical sensitivity tests revealed that the impendance contrast between the clays and the compact, cemented, alluvial layers was large enough to generate a resonance frequency peak. On an other hand, field observations, along with previous works (e.g. Monjuvent, 1973) indicate that these alluvial layers are only locally cemented. Where they are not, their mechanical parameters, especially Vs, would dramatically decrease and approach values within clays (for Vs values within alluvial sediments, see for example, Pugin et al., 2009). In such cases, the measured resonance frequency and, consequently, the base of the soft layer, would correspond to the interface between the base of non-cemented alluvial layers and the top of cemented alluvial layers and/or the Jurassic bedrock. Here again, this aspect is pointless since the aim of this work is to map the seismic substratum. Furthermore, it could partly explain the important discrepancies between the computed thicknesses and the reference cross-section (Fig. 8).

The other palaeovalley, called "Drac de Cros", recognized by geophysics and geology (Crosnier-Leconte et al., 1953; Lambert and Montjuvent, 1968; Monjuvent, 1973) is supposed to run east to the ridge, below the North-

Eastern part of the Avignonet landslide. The top of its alluvial deposits is expected to be at about 600 m asl. The location of this palaeovalley is not clear on our map. Geological observations suggest that this palaeovalley is narrower with steeper flanks than the "Drac de Sinard" one, which could explain the difficulty to see it. Here again, our estimations of the clay basement give a substratum at 530-560 m asl at the location of the expected "Drac de Cros", that is lower that geological estimate (600 m). This bias could again be explained by the fact that, the alluvial deposits are not always cemented (Monjuvent, 1973), leading to a localization of the basement that is intermediate between the top of the alluvial deposits and the top of the Jurassic bedrock. One can also notice a small East-West depression across the ridge in the middle of the Avignonet landslide that has not been reported before. However, because of the possible uncertainties of the map mentioned herebefore, we do not try to interpret it as a paleomorphological feature. In the following, we will retain only the robust features of our geophysical investigations, that are the N-S ridge and the depression related to the palaeovalley of the "Drac de Sinard".

. Beside the geophysical maps of soft layer thickness and of palaeotopography, a comparison of the Harmalière and Avignonet landslides kinematics has been done based on GPS, aerial photo and LiDAR DEM analysis. It turns out that two main differences between the two landslides are observed for the recent time: the orientation of the main sliding direction, and the level of sliding activity. Regarding the orientation it has been shown in section 3 that the Harmalière landslide is developing since 1948 along a NW-SE direction, which is significantly oblique with the expected NNW-SSE direc-

tion toward the Drac valley (before the lake filling) that can be observed, for instance, in Avignonet. The NW-SE axis also corresponds to the orientation of the "Drac de Sinard" palaeovalley below the Harmalière slide, suggesting that the orientation of the Harmalière landslide might be controlled by the palaeotopography. Regarding the level of sliding activity, a first observation is that the northern part of the Harmalière headscarp is moving to the North starting to erode the southern flank of the Avignonet slide. Secondly, GPS measurements and analysis of digital photographs, back to 1948, reveal that Harmalières main slide body is far more active than the Avignonet one: there are regression of the headscarp of several m per year being accompanied by rapid evolution of the denuded area (that are not observed on Avignonet since 60 years) and sliding velocity than can exceed 1 m/year, whereas, in Avignonet, the 11 years GPS data do not show velocity exceeding 15cm/year. These observations are consistent with the morphology of the landslides, especially the roughness, shown by the Lidar DEM which reflects more long-term activity. In Avignonet there is a gradient of displacement from the uppermost sliding clays, showing displacements of about 1-2cm/year, up to the toe of the clay mass with 10-13cm/year where the clay thickness are less than a few tens of meters (around 30m). Downward, outcrops of alluvial layer or of Jurassic bedrock do not show sliding processes. On a W-E profile along the Avignonet slide, Jongmans et al. (2009) have observed a negative correlation between the sliding velocity and the Vs values of the first 5 m suggesting a downward increasing deformation state of this clay material. They also found evidence for a slip surface at about 40 m depth within the clay confirming previous hypothesis done from inclinometric data (Blanchet, 1988;

Lorier and Desvarreux, 2004). When comparing these observations with the position of the ridge in the palaeotopography, one can be inclined to think that, here also, there is a palaeotopographic control over the kinematics: the ridge of hard layers along the eastern part of the Avignonet landslide acts as a buttress that could mechanically prevent the slide from rapid evolution as observed in Harmalière (Fig. 5).

. However, the hypothesis of a palaeotopography control over the landslide kinematics has to be discussed taking into account a longer time interval than the last 60 years of observation on which it is based. This perspective arises several questions: is the present-day kinematics, in progress since at least 1948, representative of the long term evolution of the two landslides (i.e. over several thousands of years)? If the palaeotopography controls the kinematics, what is its long term impact on the landslide morphology? One may argue that each landslide has its own evolution that consists in successive phases of slow movement (like in Avignonet today), followed by rapid events (like in Harmalière today). In this case, the present-day situation could have been the reverse at some periods in the past: an active Avignonet slide and a quiet Harmalière slide. Then, the supposed relationships between kinematics and palaeotopography would be just a coincidence or negligible.

. To address this issue, morphological parameters can be considered that may reflect the relative long term level of activity of the two landslides. The area of the Avignonet landslide is larger than in Harmalière. However, as noticed in section 2, the maximum distance to the Drac river is similar. This suggests a similar average speed of regression of the headscarps, if we do the reasonable

hypothesis that erosion processes start at the same time for the two nearby landslides, when the Drac started to incise into the glaciolacustrine deposits.

Note that, in this discussion, we will not try to use absolute time to estimate incision or erosion rates, because the timing of the beginning of the Drac incision is still debated. Some authors favor a last Würm maximum at 50-40 Ka (Monjuvent, 1973; Nicoud et al., 2002) and others at 30-20 Ka coincident with the LGM (Brocard, 2003; Brocard et al., 2003). The volume of eroded clays can be also considered. As described in section 2, it can be assumed that, at the end of the last Würm maximum, the glacio-lacustrine clay material formed a flat plateau culminating at about 750 m asl on top of which were deposited an additional 50 m of moraines as far as the south of the village of Sinard (Figs. 1 and 2; Monjuvent, 1973; Antoine et al., 1981). The eroded volume of material can be calculated by subtracting the Lidar DEM from this 800 m asl surface over the area below which clay are present for each landslide. This gives about 436 million of m^3 for Avignonet and 340 million of m^3 for Harmalière (for comparison, during the 1981 main Harmalière mudflow, 250000 m^3 went into the lake (Blanchet, 1988) but more materials were mobilized that accumulated at the bottom of the slide above the lake). If we divide theses values by the landslide area, it gives an average of 157 m of eroded clay material per m^2 for Avignonet and 195 m per m^2 for Harmalière, suggesting a higher average long-term activity for Harmalière. However, one cannot say if, for instance, these values correspond to very large events closely related in a short period of time (with the rest of the time a lower activity of the slide) or, in contrast, if they are representative of continuous evolution of the slides. The DEM morphology analysis has

shown that there is a contrast in roughness between the two landslides that suggests (with the mapping of the evolution of the denuded area) that the Harmalière slide is more active than the Avignonet one. However it can be observed within the Harmalière slide that a short term event like the 1981 mudflow and its subsequent events can change the small-scale roughness and vegetation cover of the slopes: the 1981 active body shows a visible roughness contrast with the surrounding areas of the slide. Regarding the Harmalière headscarp regression over the Avignonet slide, it seems to reflect only a recent evolution because it does not significantly modify the regular headscarp curve of the Avignonet slide. Furthermore, the observed speed of the Harmalière's headscarp regression since 1981, at about 10m/year, is not sustainable over the long term. In brief, all these morphological criteria do not seem very reliable for reflecting significant differences in kinematics of the long term (thousands of years) evolution of the slides.

. Physical mechanisms responsible of the laminated clays instability, has also to be taken into account in the analysis. It has been shown by several authors that, for the Trièves laminated clays, natural slope become instable when exceeding 6 to 8 $^\circ$ (Antoine et al., 1981, 1991; Giraud et al., 1991). According to Antoine et al. (1981), three main types of sliding are frequently observed: **1)** sliding of the vegetative cover (thickness less than 0.5 m) over the clays; **2)** creeping of a whole top clay layer (thickness 0-6 m) associated with localized and superficial mudflow; **3)** sliding of mass of clay over a slip surface (thickness up to 50 m), than can evolve into a mudflow like in Harmalire in 1981 with velocities that can reach several m/h.

. According to these processes, the palaeotopography should have an effect onto landslide activity when the clays thickness is lower than 50 m except if the material of the substratum has a significant impact on the hydrogeological conditions, for instance by draining water and influencing the water table. In Avignonet, analysis of piezometric data done so far, do not provide evidence of such an effect. Considering **1)** the present day topographic profile along the main slope direction of the Avignonet slide, **2)** the position of the ridge at about 700 m west to the Drac valley with a highest point at about 620m and **3)** the initial level surface, at around 800m asl, in which the Drac started to incise, one can say that the possible effects of the palaeotopography on the landslide activity did not start at the beginning of the slide's life and may be relatively recent in the slide histories. That could explain why there is no clear evidence of long term difference of activities between the two landslides. When the deep slip surfaces started to reach the clay basement, the development of new deeper slip surface has been influenced because the basement prevents them to go deeper, as it has been expected if no ridge were present. This certainly causes a slowing of their evolution. In Avignonet, Blanchet (1988) and Jongmans et al. (2009) proposed several hypotheses about the geometry of a deep slip surface at about 50m identified from inclinometric data. These geometries are influenced by the basement in their lowest part, suggesting that the Avignonet landslide activity may have been recently slow down by the palaeotopography. The fact that the GPS velocities are the highest in the lowest part near the ridge is interpreted as being due to more intensive superficial creep at the toe of the slide. In the Harmalière slide, no inclinometric data are available. However, applying

similar reasoning, one can say that the situation where the deep slip surfaces reach the clay basement has not started on the NW-SE profiles along which the slide is developing (Fig. 9). If, instead, we consider an E-W profile in the middle of the Harmalière slide, the situation looks more similar to the Avignonet case. This could explain why the Harmalière slide is developing along an NW-SE direction and why it has recently shown a highest activity than in Avignonet.

. Consequently, we propose that palaeotopography is a significant controlling factor of the Harmalière and Avignonet landslide evolutions, acting as a mechanical buttress against the development of slip surfaces in the clays. Paleotopography may also have another impact (not investigated in this study), that is an influence on the drainage condition of the two landslides because paleotopography is responsible of large permeability heterogeneities due to the presence of alluvial deposits in the palaeovalleys.

6. Conclusion

. The two adjacent landslides of Avignonet and Harmalière have been studied following an original multidisciplinary approach based on geodetic (GPS, digital photographs), remote sensing (LiDAR), and ground geophysics (ambient noise measurements). The aim was to understand the differential kinematics, motion directions and morphology that characterize these landslides located in the same geotechnical setting.

GPS measurements and digital photographs reveal that the difference in kinematics between the two earthslides can be tracked back to 60 years ago at least. The Avignonet slide is mainly directed towards the East (N 100 $^\circ$ E)

while Harmalière is mainly oriented towards SE. The LiDAR scan map illustrates this differential motion and morphology between the two slides and highlights that the Harmalière slide is still presently much more active than the Avignonet one.

A ground geophysical prospecting based on ambient noise measurements allowed to record the resonance frequencies at different locations. These measured resonance frequencies where turned into soft sediments thicknesses. Finally, a map depicting the base of the clays was computed. It indicates that the basement is very irregularly shaped with strong lateral E-W variations over 150 m. This map confirms previous field and geophysical observations that revealed a westward thickening of the clays. This map also reveals the presence of a N-S ridge of hard sediments (Jurassic bedrock and/or compact alluvial layers) on the eastern side of the Avignonet landslide. This ridge disappears when approaching the Harmalière landslide and makes place to what can be interpreted like a NW-SE oriented palaeovalley of the river Drac. It is proposed that the ridge could act as a butress which could mechanically prevent the Avignonet landslide from evolving as fast as the Harmalière one. Furthermore the NW-SE palaeovalley located under the Harmalière landslide corresponds to the motion direction of the slide. It is then finally proposed that the slides different behaviours are partly controlled by the palaeotopographic setting of lake Trièves.

This approach reveals to be a quick and relatively low-cost way to characterize the geomorphological setting of this sedimentary basin over an important area of $5\,\mathrm{km}^2$ by building a geometrical framework for lansdlide characterization within fine-grained soft-sediments.

Acknowledgements

This work was supported by the European project "Mountain Risks" (Marie Curie program) and the Department of Isère through the Pôle Grenoblois des Risques Naturels. The authors thank F. Renalier, Y. Orengo and M. Wathelet for their participation to the seismic measurements.

7. References

References

Abellan, A., Vilaplana, J. M., Martinez, J., 2006. Application of a long-range terrestrial laser scanner to a detailed rockfall study at Vall de Nuria (Eastern Pyrenees, Spain). Engineering Geology 88, 136–148.

Antoine, P., Giraud, A., Montjuvent, G., 1981. Les argiles litées du Trièves (Isère) ; conditions de gisement et exemples de propriétés géotechniques. Bulletin de la Société Géologique de France (7), t. XXIII (2), 117–127.

Antoine, P., Monnet, J., Rai, N. E., Moulin, C., Mériaux, P., 1991. Résultats de cinq années d'auscultation sur un glissement dans les argiles glacio-lacustres du Trièves (Sud-Est de la France). In: 6th International Symposium on Landslides. Balkema, Rotterdam.

Bard, P.-Y., 1998. Microtremor measurements: a tool for site effect estimation? In: Irikura, K., Kudo, K., Okada, H., Sasatani, T. (Eds.), The Effects of Surface Geology on Seismic Motion. Balkema, Rotterdam, pp. 1251–1279.

Blanchet, F., 1988. Etude géomécanique de glissements de terrain dans les argiles glaciolacustres de la vallée du Drac. Ph.D. thesis, Université Joseph Fourier, Grenoble, France, Grenoble, France.

Bonci, L., Bozzano, F., Calcaterra, S., Eulilli, V., Ferri, F., Gambino, P., Manuel, M. R., Martino, S., Scarascia Mugnozza, G., 2004. Geological control on large seismically induced landslides: the case of Cerda (Southern

833 Italy). In: Proceedings of the 9th International Symposium on Landslides.
834 pp. 985–991.

835 Bonnefoy-Claudet, S., Cornou, C., Bard, P.-Y., Cotton, F., Moczo, P., Kris-
836 tek, J., Fäh, D., 2006. H/V ratio: a tool for site effects evaluation. Results
837 from 1-D noise simulations. Geophysical Journal International 167, 827–
838 837.

839 Bozzano, F., Lenti, L., Martino, S., Paciello, A., Scarascia Mugnozza, G.,
840 2008. Self-excitation process due to local seismic amplification responsible
841 for the reactivation of the Salcito landslide (Italy) on 31 October 2002.
842 Journal of Geophysical Research 113, B10312.

843 Briese, C., Pfeifer, N., Dorninger, P., 2002. Applications of the robust inter-
844 polation for DTM determination. In: IAPSIS XXXIV. Vol. 3A. pp. 55–61.

845 Brocard, G. Y., Van Der Beek, P. A., Bourlès, D. L., Siame, L. L., Mugnier,
846 J.-L., 2003. Long-term fluvial incision rates and postglacial river relaxation
847 time in the French Western Alps from 10Be dating of alluvial terraces
848 with assessment of inheritance, soil development and wind ablation effects.
849 Earth and Planetary Science Letters 209, 197–214.

850 Brocard, G. Y., 2003. Origine, variabilité spatio-temporelle et signature mor-
851 phologique de l'incision fluviatile dans les Alpes dauphinoises (SE France).
852 Géologie Alpine, Mémoire H.S. 43.

853 Brückl, E., Brunner, F. K., Kraus, K., 2006. Kinematics of a deep-seated
854 landslide derived from photogrammetric, GPS and geophysical data. En-
855 gineering Geology 88 (3-4), 149–159.

856 Chatelain, J.-L., Guéguen, P., Guillier, B., Fréchet, Bondoux, F., Sarrault,
857 J., Sulpice, P., Neuville, J. M., 2000. Cityshark: A user-friendly instrument
858 dedicated to ambient noise (microtremor) recording for site and building
859 response studies. Seismological Research Letters 71, 698–703.

860 Clark, P. U., Dyke, A. S., Shakun, J. D., Carlson, A. E., Clark, J., Wohlfarth,
861 B., Mitrovica, J. X., Hostetler, S. W., McCabe, A. M., 2009. The Last
862 Glacial Maximum. Science 325 (5941), 710–714.

863 Corsini, A., Borgatti, L., Coren, F., Vellico, M., 2007. Use of multitemporal
864 airborne LiDAR surveys to analyse postfailure behaviour of earthslides.
865 Canadian Journal of Remote Sensing 33 (2), 116–120.

866 Crosnier-Leconte, J., Bordet, C., Duffaut, P., 1953. Séparation de deux an-
867 ciens lits successifs dans la vallée du Drac à Monteynard (Isère). Comptes-
868 Rendus Sommaires de la Société Géologique de France 12, 221–223.

869 Debelmas, J., 1967. La Chapelle-en-Vercors. In: Carte géologique de la
870 France au 1/50000. BRGM Éditions, Orlans, France.

871 Delacourt, C., Allemand, P., Bertier, E., Raucoules, D., Casson, B., Grand-
872 jean, P., Pambrun, C., Varel, E., 2007. Remote-sensing techniques for
873 analysing landslide kinematics: a review. Bulletin de la Société Géologique
874 de France 178 (2), 89–100.

875 Delgado, J., López Casado, C., Estévez, A., Giner, J., Cuenca, A., Molina,
876 S., Aug. 2000. Mapping soft soils in the Segura river Valley (SE Spain);
877 a case study of microtremors as an exploration tool. Journal of Applied
878 Geophysics 45 (1), 19–32.

879 Deparis, J., Fricourt, B., Jongmans, D., Villemin, T., Effendiantz, L., Mathy,
880 A., 2008. Combined use of geophysical methods and remote techniques for
881 characterizing the fracture network of a potential unstable cliff site (the
882 'Roche du Midi', Vercors massif, France). Journal of Geophysical Engi-
883 neering 5, 147–157.

884 Eilertsen, R. S., Hansen, L., Bargel, T. H., Solberg, I.-L., 2008. Clay slides
885 in the Mlselv valley, northern Norway: Characteristics, occurrence, and
886 triggering mechanisms. Geomorphology 93 (3-4), 548–562.

887 Fruneau, B., Achache, J., Delacourt, C., 1996. Observation and modelling of
888 the Saint-Étienne-de-Tinée landslide using SAR interferometry. Tectono-
889 physics 265, 181–190.

890 Giraud, A., Antoine, P., Van Asch, T. W. J., Nieuwenhuis, J. D., 1991.
891 Geotechnical problems caused by glaciolacustrine clays in the French Alps.
892 Engineering Geology 31, 185–195.

893 Glenn, N. F., Streutker, D. R., Chadwick, D. J., Thackray, G. D., Dorsch,
894 S. J., Jan. 2006. Analysis of LiDAR-derived topographic information for
895 characterizing and differentiating landslide morphology and activity. Geo-
896 morphology 73 (1-2), 131–148.

897 Green, A. G., Maurer, H., Spillmann, T., Heincke, B., Willenberg, H., 2007.
898 High-resolution geophysical techniques for improving hazard assessments
899 of unstable rock slopes. The Leading Edge 25 (3), 311–316.

900 Guéguen, P., Cornou, C., Garambois, S., Banton, J., Jan. 2007. On the Lim-
901 itation of the H/V Spectral Ratio Using Seismic Noise as an Exploration

902 Tool: Application to the Grenoble Valley (France), a Small Apex Ratio
903 Basin. Pure and Applied Geophysics 164 (1), 115–134.

904 Guillier, B., Cornou, C., Kristek, J., Bonnefoy-Claudet, S., Bard, P., Fah,
905 D., , Moczo, P., 2006. Simulation of seismic ambient vibrations: does the
906 H/V provide quantitative information in 2D-3D structure ? In: ESG2006.
907 Grenoble.

908 Haskell, N. A., 1960. Crustal reflexion of plane Sh waves. Journal of Geo-
909 physical Research 65, 4147–4150.

910 Heincke, B., Maurer, H., Green, A. G., Willenberg, H., Spillmann, T.,
911 Burlini, L., 2006. Characterizing an unstable mountain slope using shallow
912 2D and 3D seismic tomography. Geophysics 71 (6), B241–B256.

913 Huff, W. D., 1974. Mineralogy and provenance of Pleistocene lake clay in an
914 alpine region. Geological Society of America Bulletin 85, 1455–1460.

915 Ibs-von Seht, M., Wohlenberg, J., 1999. Microtremor measurements used to
916 map thickness of soft sediments. Bulletin of the Seismological Society of
917 America 89 (1), 250–259.

918 IPF, 2004. Software SCOP++, http://www.ipf.tuwien.ac.at/products/produktinfo/scop/scop_dtm.

919 Jongmans, D., Bièvre, G., Schwartz, S., Renalier, F., Beaurez, N., 2009. Geo-
920 physical investigation of the large Avignonet landslide in glaciolacustrine
921 clays in the Trièves area (french Alps). Engineering Geology 109, 45–56.

922 Jongmans, D., Garambois, S., 2007. Geophysical investigation of landslides
923 : a review. Bulletin de la Société Géologique de France 178 (2), 101–112.

924 Kimura, H., Yamaguchi, Y., 2000. Detection of landslide areas using satellite
925 radar interferometry. Photogrammetric engineering and remote sensing 66,
926 337–344.

927 Kitanidis, P. K., 1997. Introduction to Geostatistics: Applications in Hydro-
928 geology. Cambridge University Press, Cambridge.

929 Koller, M. G., Chatelain, J.-L., Guillier, B., Duval, A.-M., Atakan, K., La-
930 cave, C., Bard, P.-Y., 2004. Practical user guidelines and software for the
931 implementation of the H/V ratio technique: measuring conditions, pro-
932 cessing method and results interpretation. In: Proceedings of the 13th
933 world conference in earthquake engineering, Vancouver, Canada.

934 Konno, K., Ohmachi, T., 1998. Ground-motion characteristics estimated
935 from spectral ratio between horizontal and vertical components of mi-
936 crotremor. Bulletin of the Seismological Society of America 88 (1), 228–241.

937 Lambert, A., Montjuvent, G., 1968. Quelques vues nouvelles sur l'histoire
938 quaternaire de la vallée du Drac (note préliminaire). Géologie Alpine 44,
939 117–138.

940 Lapenna, V., Lorenzo, P., Perrone, A., Piscitelli, S., Rizzo, E., Sdao, F.,
941 May 2005. 2D electrical resistivity imaging of some complex landslides in
942 Lucanian Apennine chain, southern Italy. Geophysics 70 (3), B11–B18.

943 Le Roux, O., Schwartz, S., Gamond, J.-F., Jongmans, D., Tricart, P., Se-
944 brier, M., 2008. Interaction between tectonic and erosion processes on the
945 morphogenesis of an Alpine valley: geological and geophysical investiga-

946 tions in the lower Romanche valley (Belledonne massif, western Alps).
947 International Journal of Earth Sciences, 1437–3254.

948 Lorier, L., Desvarreux, P., 2004. Glissement du Mas d'Avignonet, commune
949 d'Avignonet. In: Proceedings of the workshop Ryskhydrogeo, Program
950 Interreg III, La Mure (France). p. 8 p.

951 McKean, J., Roering, J., 2004. Objective landslide detection and surface
952 morphology mapping using high-resolution airborne laser altimetry. Geo-
953 morphology 57 (3-4), 331–351.

954 Méneroud, J.-P., Duval, A.-M., Vidal, S., Fréchet, J., Gamond, J.-F., Beck,
955 C., Tardy, M., Bard, P.-Y., Barnichon, E., Gaboriaud, J.-M., 1995.
956 Franchissement de l'Ebron, Etude de l'aléa sismique local. Tech. Rep.
957 93/95666/74, CETE Méditerranée.

958 Méric, O., Garambois, S., Malet, J.-P., Cadet, H., Gueguen, P., Jongmans,
959 D., 2007. Seismic noise-based methods for soft-rock landslide characteriza-
960 tion. Bulletin de la Societe Geologique de France 178 (2), 137–148.

961 Metternicht, G., Hurni, L., Gogu, R., 2005. Remote sensing of landslides:
962 An analysis of the potential contribution to geospatial systems for hazard
963 assessment in mountainous environments. Remote Sensing of Environment
964 98, 284–303.

965 Monjuvent, G., 1973. La transfluence Durance-Isère. Essai de synthèse du
966 Quaternaire du bassin du Drac (Alpes françaises). Géologie Alpine 49, 57–
967 118.

968 Moulin, C., Chapeau, C., 2004. Le glissement de la Salle en Beaumont (Isère).
969 In: Proceedings of the workshop Ryskhydrogeo, Program Interreg III, La
970 Mure (France). p. 9 p.

971 Moulin, C., Robert, Y., 2004. Le glissement de l'Harmalière sur la commune
972 de Sinard. In: Proceedings of the workshop Ryskhydrogeo, Program Inter-
973 reg III, La Mure (France). p. 11 p.

974 Nicoud, G., Royer, G., Corbin, J.-C., Lemeille, F., Paillet, A., 2002. Creuse-
975 ment et remplissage de la vallée de lIsère au Quaternaire récent. Apports
976 nouveaux du forage GMB1 (1999) dans la région de Grenoble (France).
977 Géologie de la France 4, 39–49.

978 Oppikofer, T., Jaboyedoff, M., Keusen, H.-R., 2008. Collapse at the eastern
979 Eiger flank in the Swiss Alps. Nature Geoscience 1, 531–535.

980 Perrone, A., Zeni, G., Piscitelli, S., Pepe, A., Loperte, A., Lapenna, V.,
981 Lanari, R., 2006. Joint analysis of SAR interferometry and electrical re-
982 sistivity tomography surveys for investigating ground deformation: the
983 case-study of Satriano di Lucania (Potenza, Italy). Engineering Geology
984 88 (3-4), 260–273.

985 Pugin, A. J.-M., Pullan, S. E., Hunter, J. A., Oldenborger, G. A., 2009.
986 Hydrogeological prospecting using P- and S-wave landstreamer seismic re-
987 flection methods. Near Surface Geophysics 7, 315–327.

988 Renalier, F., Jongmans, D., Bièvre, G., Schwartz, S., Orengo, Y., 2007.
989 Characterisation of a landslide in clay deposits using Vs measurements.

In: Near Surface 2007, EAGE meeting, 03-04 September 2007, Istanbul, Turkey.

Roch, K. H., Chwatal, E., Brückl, E., 2006. Potential of monitoring rock fall hazards by gpr: considering as example of the results of Salzburg. Landslides 3, 87–94.

Rosser, N. J., Petley, D. N., Lim, M., Dunning, S. A., Allison, R. J., 2005. Terrestrial laser scanning for monitoring the process of hard rock coastal cliff erosion. Quarterly Journal of Engineering Geology 38, 363–375.

Rott, H., Scheuchl, B., Siegel, A., Grasemann, B., 1999. Monitoring very slow slope motion by means of SAR interferometry: A case study from a mass waste above a reservoir in the Ötztal Alps, Austria. Geophysical Research Letters 26, 1629–1632.

Schulz, W. H., 2007. Landslide susceptibility revealed by LiDAR imagery and historical records, Seattle, Washington. Engineering Geology 89 (1-2), 67–87.

Shepard, M. K., Campbell, B. A., Bulmer, M. H., Farr, T. G., Gaddis, L. R., Plaut, J. J., 2001. The roughness of natural terrain: A planetary and remote sensing perspective. Journal of Geophysical Research 106 (E12), 32777–32795.

Squarzoni, C., Delacourt, C., Allemand, P., 2003. Nine years of spatial and temporal evolution of the La Valette landslide observed by SAR interferometry. Engineering Geology 68, 53–66.

1012 Strozzi, T., Farina, P., Corsini, A., Ambrosi, C., Thüring, M., Zilger, J., A.,
1013 W., Wegmüller, U., Werner, C., 2005. Survey and monitoring of landslide
1014 displacements by means of L-band satellite SAR interferometry. Landslides
1015 2, 193–201.

1016 Thoma, D. P., Guptab, S. C., Bauerc, M. E., Kirchoff, C. E., 2005. Air-
1017 borne laser scanning for riverbank erosion assessment. Remote Sensing of
1018 Environment 95, 493–501.

1019 Uebayashi, H., 2003. Extrapolation of Irregular Subsurface Structures Us-
1020 ing the Horizontal-to-Vertical Spectral Ratio of Long-Period Microtremors.
1021 Bulletin of the Seismological Society of America 93 (2), 570–582.

1022 Vallet, J., Skaloud, J., 2004. Development and experiences with a fully-digital
1023 handheld mapping system operated from helicopter. The International
1024 Archives of the Photogrammetry, Remote Sensing and Spatial Informa-
1025 tion Sciences XXXV (Commission 5), Part B.

1026 Van den Eeckhaut, M., Poesen, J., Verstraeten, G., Vanacker, V., Moeyer-
1027 sons, J., Nyssen, J., Van Beek, L. P. H., Vandekerckhove, L., 2007. Use
1028 of LiDAR-derived images for mapping old landslides under forest. Earth
1029 Surface Processes and Landforms 32, 754–769.

1030 Wathelet, M., Jongmans, D., Ohrnberger, M., 2004. Surface-wave inversion
1031 using a direct search algorithm and its application to ambient vibration
1032 measurements. Near Surface Geophysics 2, 211–221.

Table 1: Root-mean-square deviations from the elevation profiles seen in Figure 5b for 2 different wavelengths (step sizes) representing the roughness at different scales. See text for details. * This value is not reliable due to the short profile length.

	A1-A2 upper Avignonet	A2-A3 lower Avignonet	H1-H2 upper Harmalière	H2-H3 lower Harmalière
Profile length (m)	577	247	874	624
Mean slope angle (°)	9.8	16.3	11.6	6.9
RMS deviation (m) small scale (10 m)	1.1	1.6	1.6	1
RMS deviation (m) large scale (100 m)	4.4	4.4*	5.4	2

Table 2: Dynamic characteristics (compressional wave velocity Vp, shear wave velocity Vs and density) used for the calculation of the theoretical resonance frequency. See text for details.

Geological unit	***Thickness (m)***	***Vp (m/s)***	***Vs (m/s)***	***Density***
Morainic colluvium	5	500	250	1.9
Moraines	0-50	1850	150-450	2
Disturbed clays	0-45	1850	150-450	2
Unidisturbed clays	0-250	1850	600-650	2
Compact alluvium	0-100	2350	1250	2
Carbonate bedrock	Halfspace	3000	2000	2.6

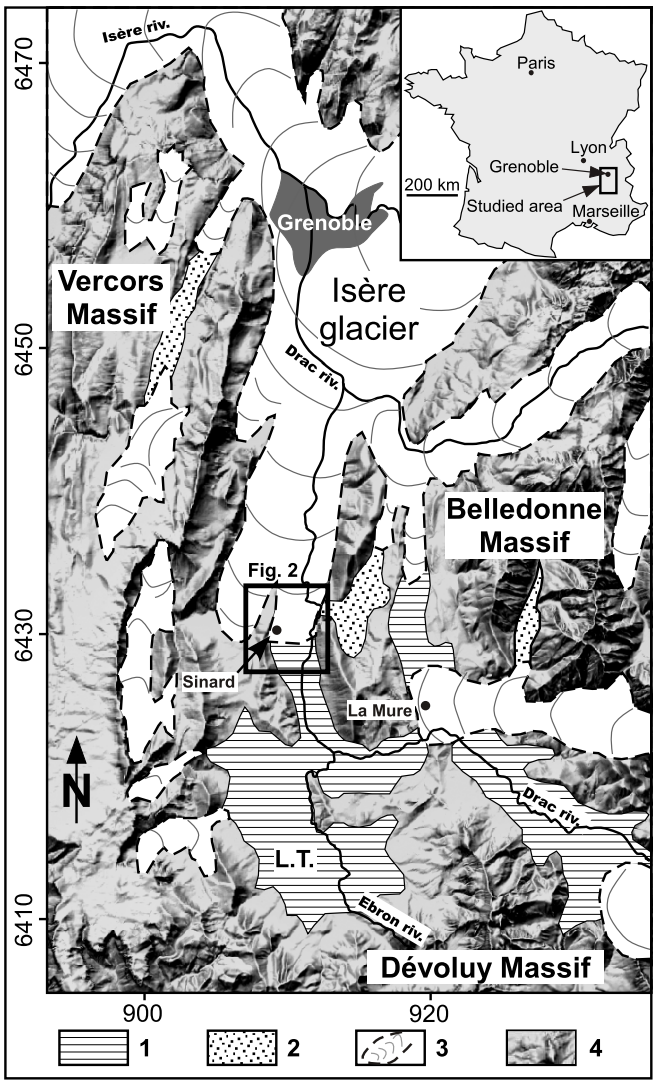

Figure 1: Location of the area and palaeogeographical map at the end of the Würm age (adapted from Monjuvent, 1973). Coordinates are kilometric and expressd in the French system Lambert-93. The black thick box shows the location of the study area and the extent of Fig. 2. 1: Laminated clay deposits in the Trièves area; 2: glaciofluvial deposits; 3: extension of the Isère Glacier at the end of the Würm age; 4: present-day topography; L.T.: lake Trièves.

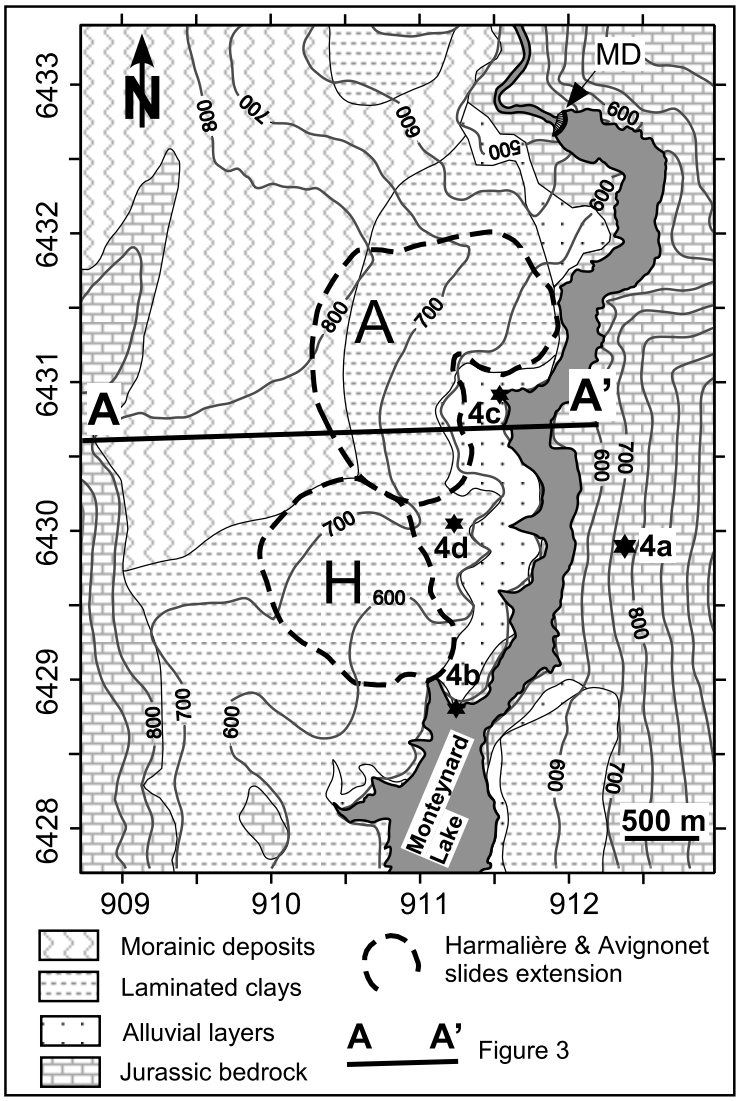

Figure 2: Geological map (location in Fig. 1) modified from Debelmas (1967) and Lambert and Montjuvent (1968). Screes and morainic colluvium have not been reported. Black stars refer to pictures in figure 4. Position of cross-section AA' of figure 3 is indicated. A: Avignonet landslide. H: Harmalière landslide. MD : Monteynard dam.

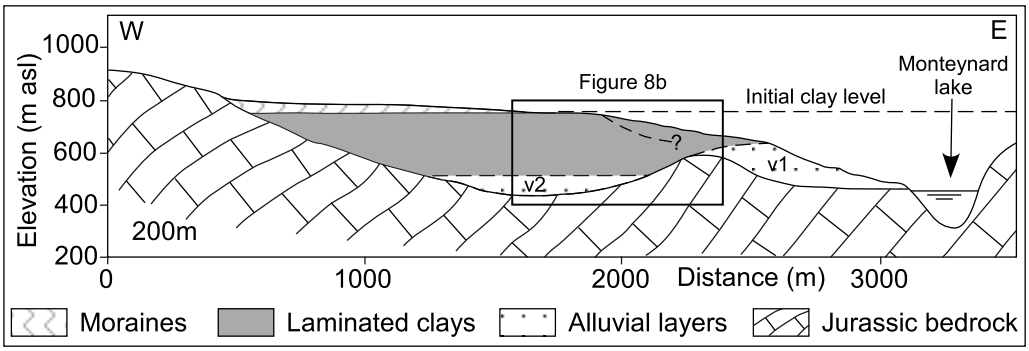

Figure 3: Geological cross section (location in Fig. 3). Screes and morainic colluvium have not been reported. v1: first palaeovalley ("Drac de Cros"). v2: second palaeovalley ("Drac de Sinard"). Initial level of laminated clays has been reported (750 m asl). Dashed line within clays depicts the lower limit of the Avignonet landslide, deduced from inclinometer data. See text for details.

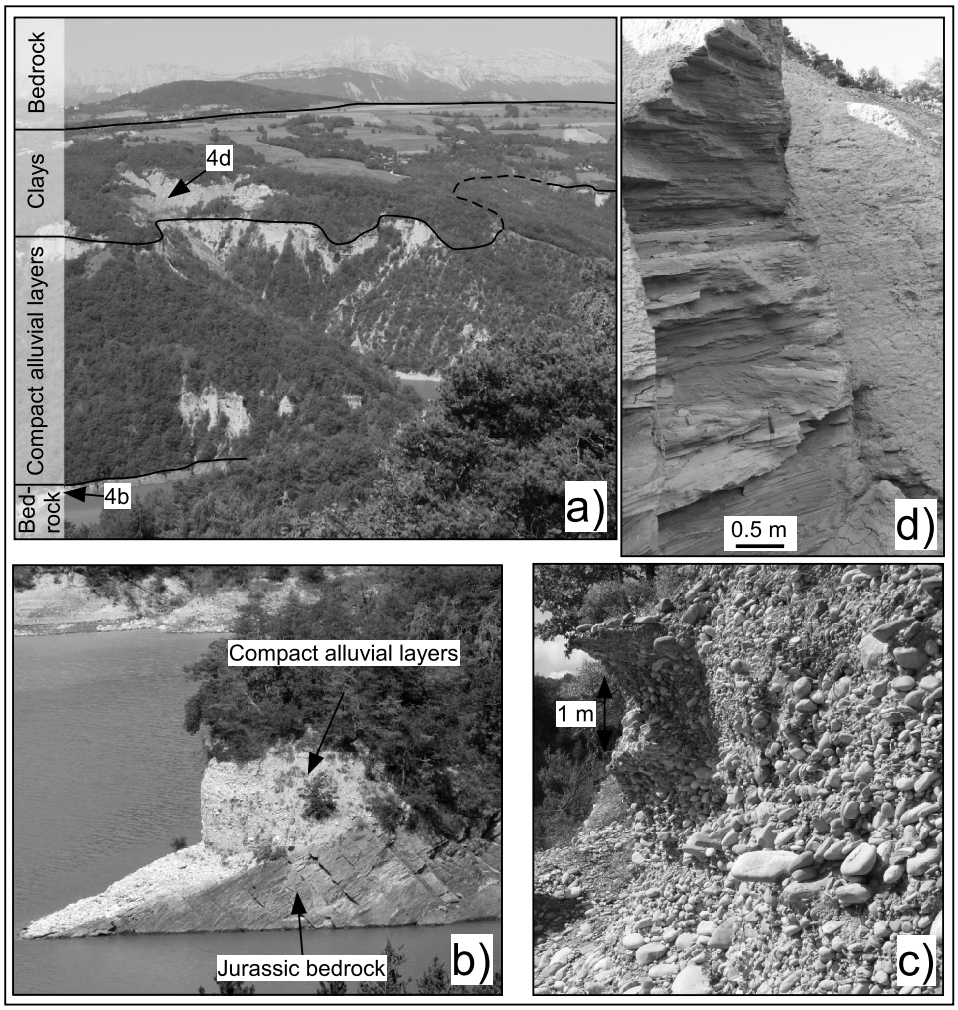

Figure 4: Outcrop pictures. **a)** General view of the Avignonet landslide from the opposite bank of lake Monteynard (picture taken from location 4a in Fig. 2); **b)** Jurassic bedrock overlain by compact, locally cemented alluvial layers constituted by hetermetric and heterogenic gravels. Present-day Drac river is at the forefront; **c)** Compact alluvial layers; **d)** laminated clays. Location of the pictures is detailed on Fig. 2

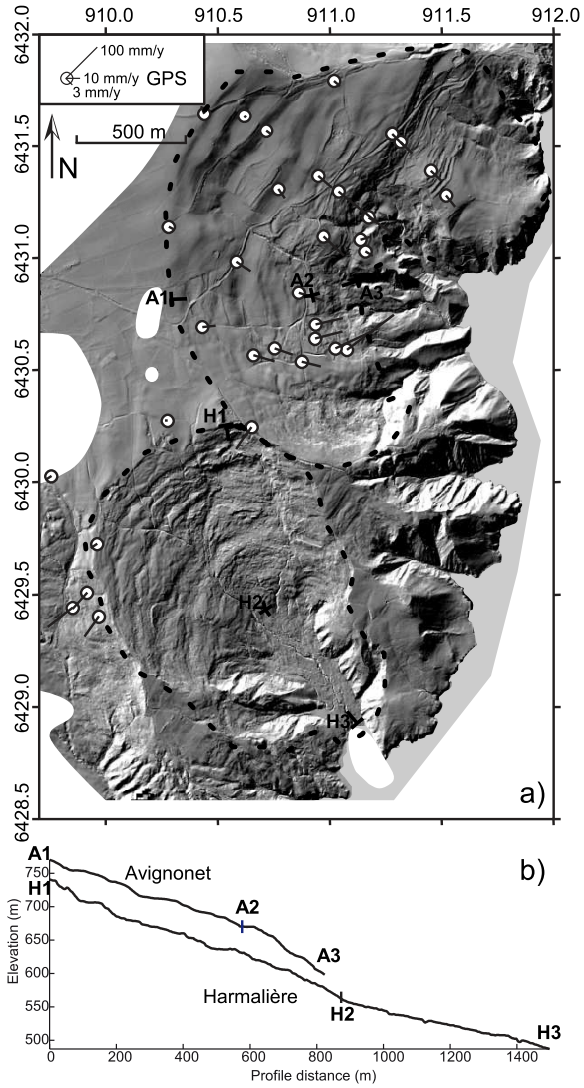

Figure 5: LidAR DEM and elevation profiles of the study area. **a)** Shaded LiDAR DEM (light direction is from NW, horizontal resolution of 2 m) covering the Avignonet (North) and Harmalière (South) landslides. Dotted lines indicate the landslide limits. White areas indicate data holes in the LiDAR coverage. The white circles show the position of the GPS points, and the thin straight lines represent the 11-years average horizontal velocity measured by GPS. A1-3 and H1-3 indicate the location of the elevation profiles. **b)** Elevation profiles through Avignonet and Harmalière with subdivisions in an upper and lower part. Profiles are 2 times vertically exaggerated.

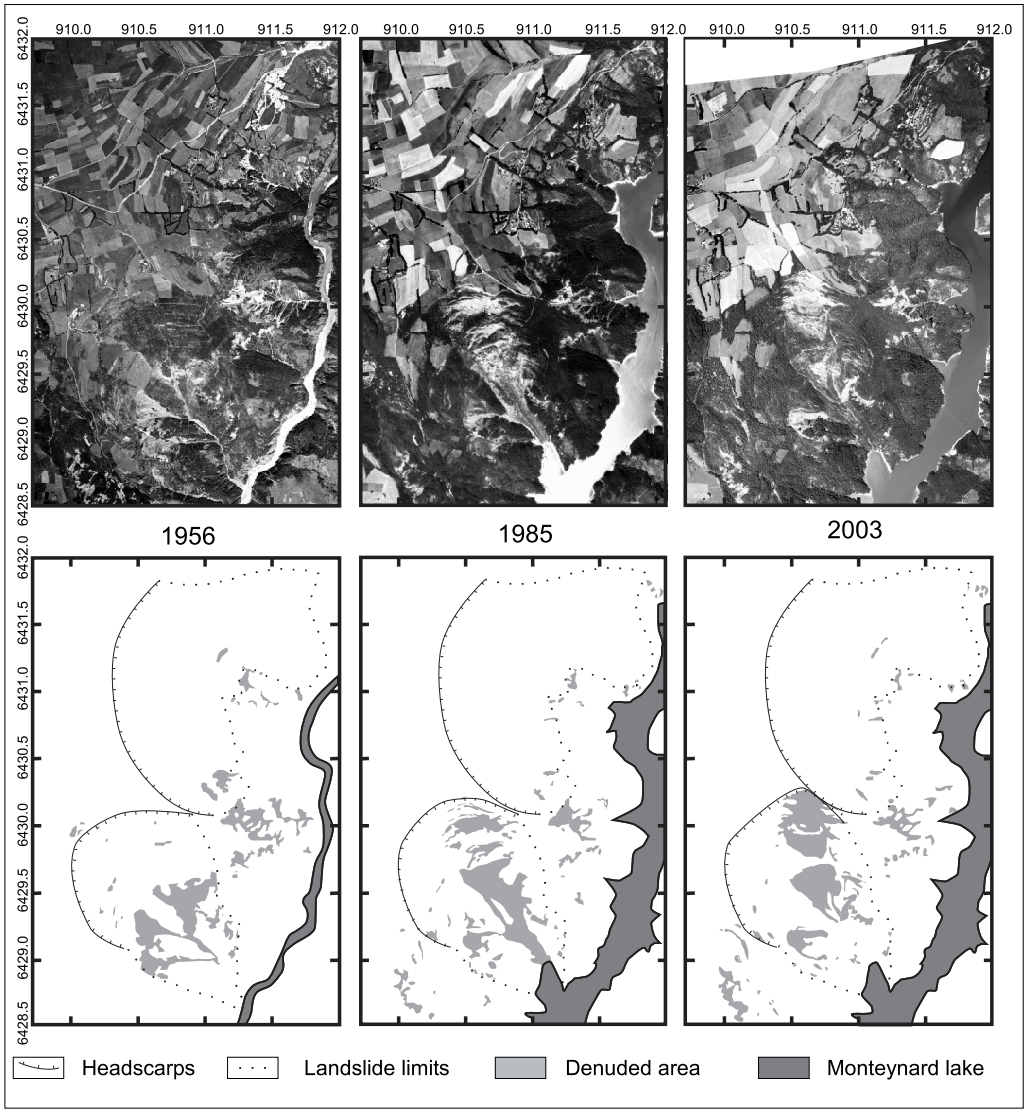

Figure 6: Top: Orthorectified aerial photos of the years 1956, 1985 and 2003. The scales of the original photos are 1:25 000, 1:30 000 and 1:25 000. Bottom: Interpretation of the corresponding aerial photo showing the denuded areas related to landslide activity. White areas are not covered by the images. In 1962 the Drac River was damed up creating the lake Monteynard shown in the photos from 1985 and 2003.

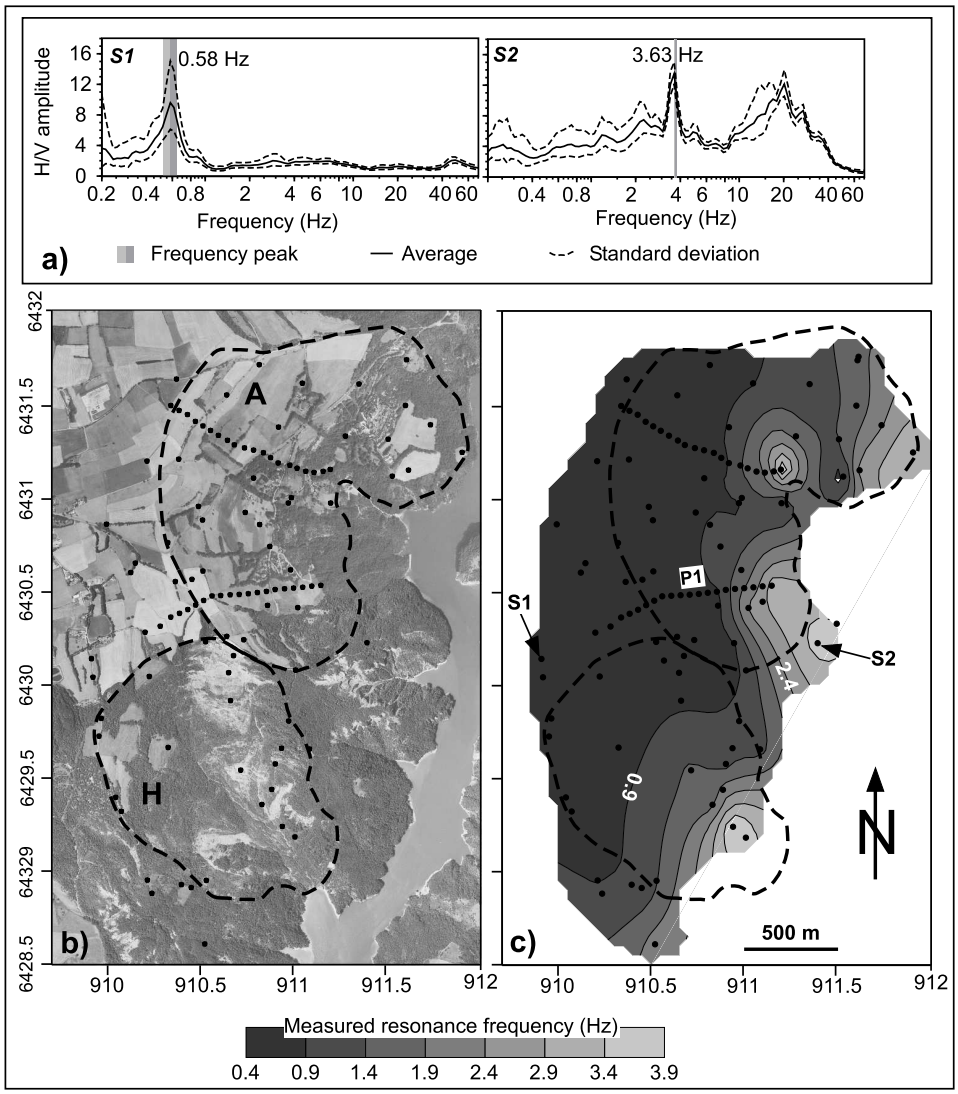

Figure 7: H/V measurements. **a)** H/V curves at points S1 and S2 (location on Fig. 7c). **b)** Location of the 104 measurement points with the landslides limits (dashed line); A: Avignonet landslide; H: Harmalière landslide. **c)** Resonance frequency map.

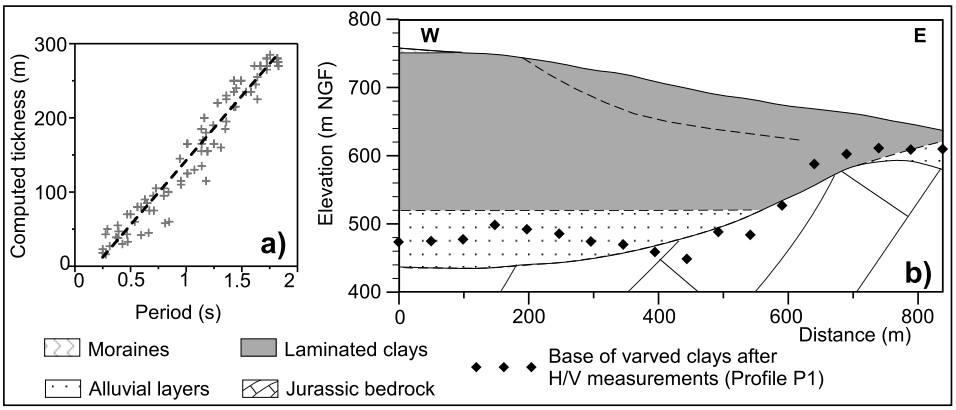

Figure 8: Frequency to thickness calibration for H/V profile P1 (location on Figs. 7b and 7c). **a)** Computed thickness as a function of the measured resonance period (inverse of the frequency) for the 104 stations. Linear regression (black dashed line) gives a determination coefficient r^2 equals to 0.95. **b)** Comparison of the geometry of the top of the Jurassic bedrock (Blanchet, 1988) and the bottom of the laminated clays after H/V measurements along profile P1 (location in Fig. 7c). Dashed line depicts the lower limit of the Avignonet landslide deduced from inclinometer data.

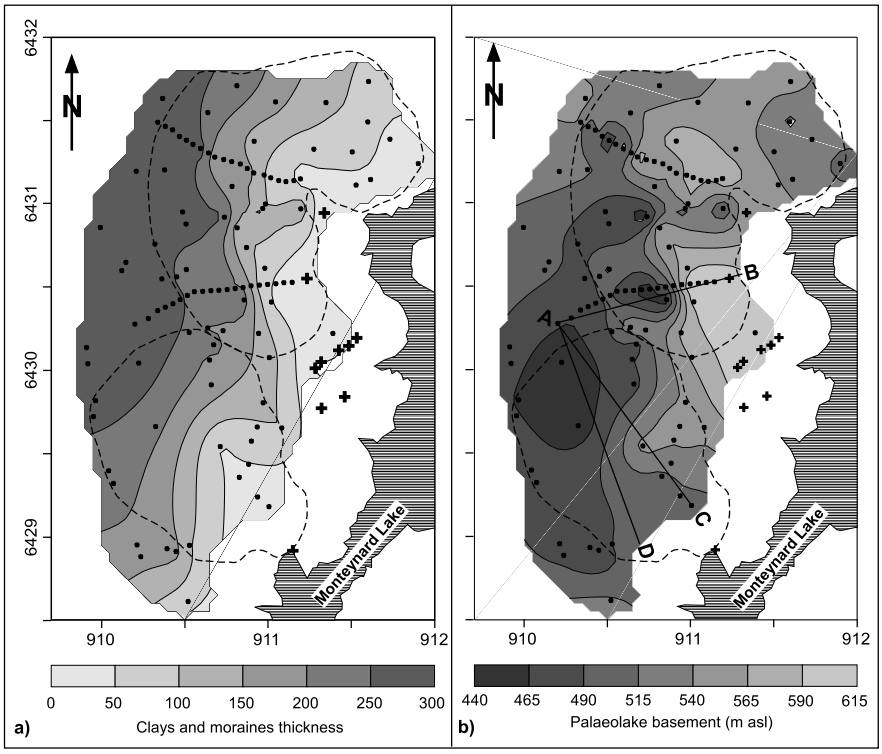

Figure 9: Soft layer thickness maps. **a)** Soft layer thickness map. The absolute error between computed and interpolated thicknesses is 5.29 %. **b)** Lake Trièves palaeotopography in the study area. The absolute error between computed and interpolated palaeotopography is 0.98 %. Dots refer to seismic measurements and crosses to field observations; dashed lines stand for Avignonet and Harmalière landslides limits.

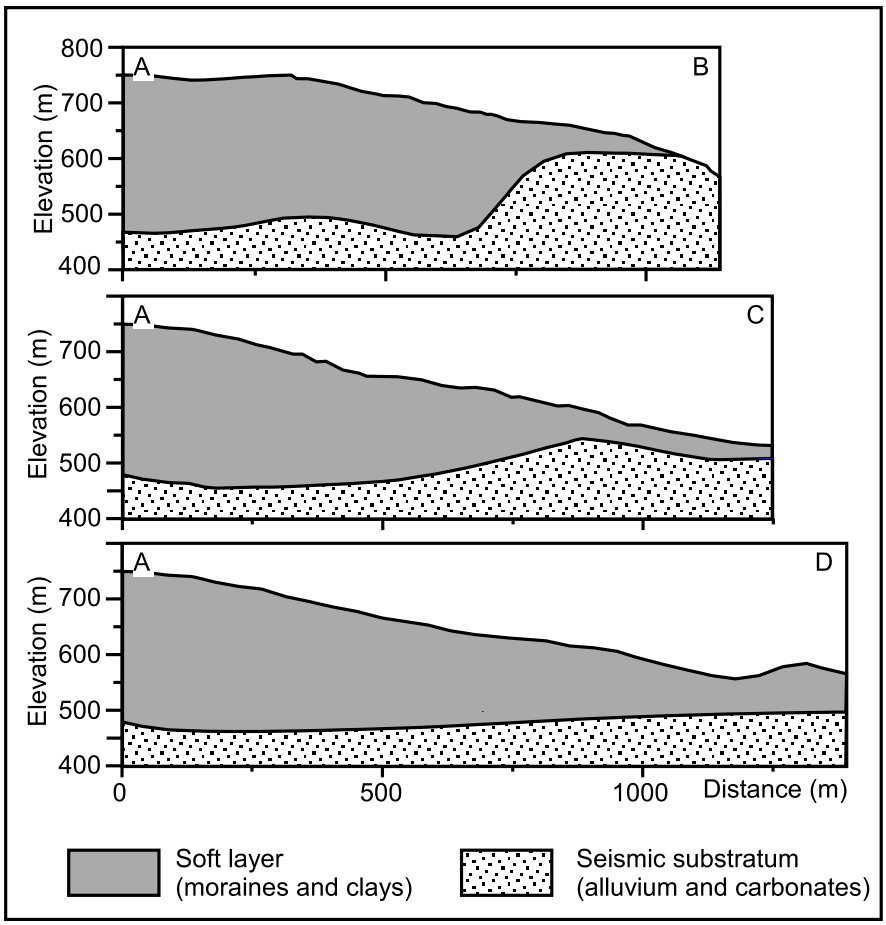

Figure 10: Cross-sections of the paleolake basement (location in Fig. 9b).

Figure 5

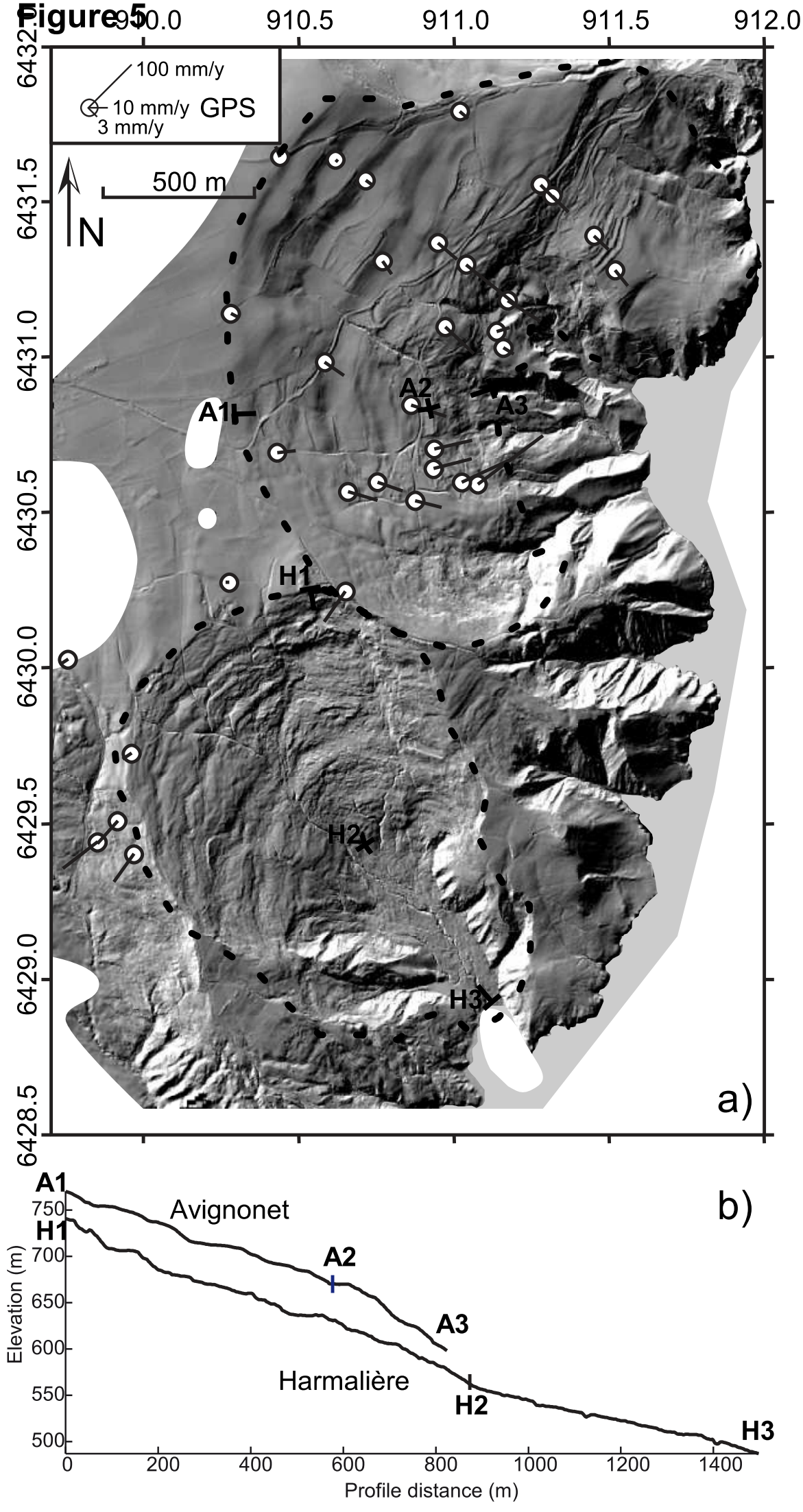
910.0
910.5
911.0
911.5
912.0
6432
6431.5
6431.0
6430.5
6430.0
6429.5
6429.0
6428.5
100 mm/y
10 mm/y
3 mm/y
GPS
500 m
N
A1
A2
A3
H1
H2
H3
a)
b)
Avignonet
Harmalière
Elevation (m)
750
700
650
600
550
500
0
200
400
600
800
1000
1200
1400
Profile distance (m)

Figure 9

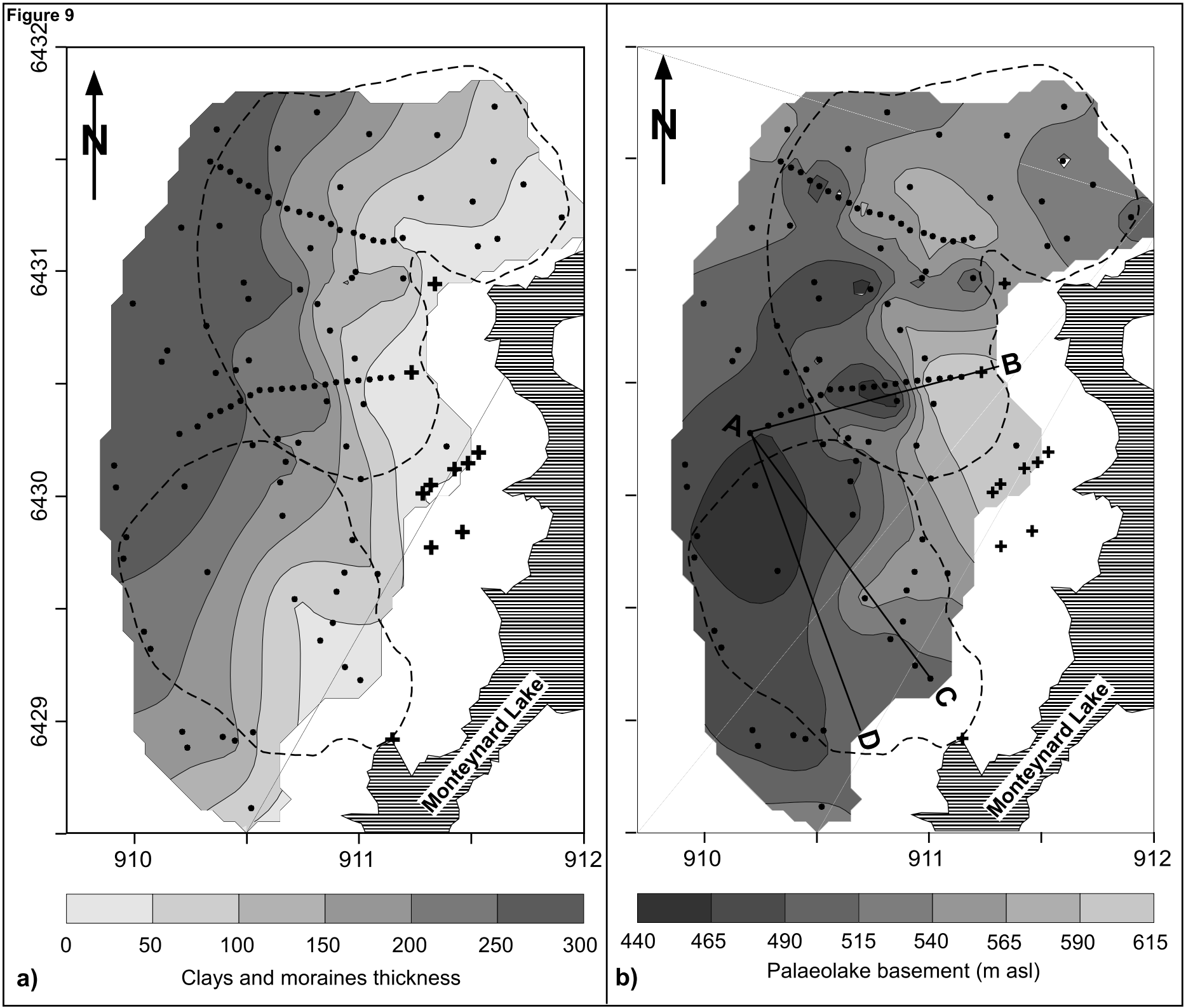
6432
6431
6430
6429
N
910
911
912
Monteynard Lake
0
50
100
150
200
250
300
a)
Clays and moraines thickness
A
B
C
D
440
465
490
515
540
565
590
615
b)
Palaeolake basement (m asl)

Figure 10

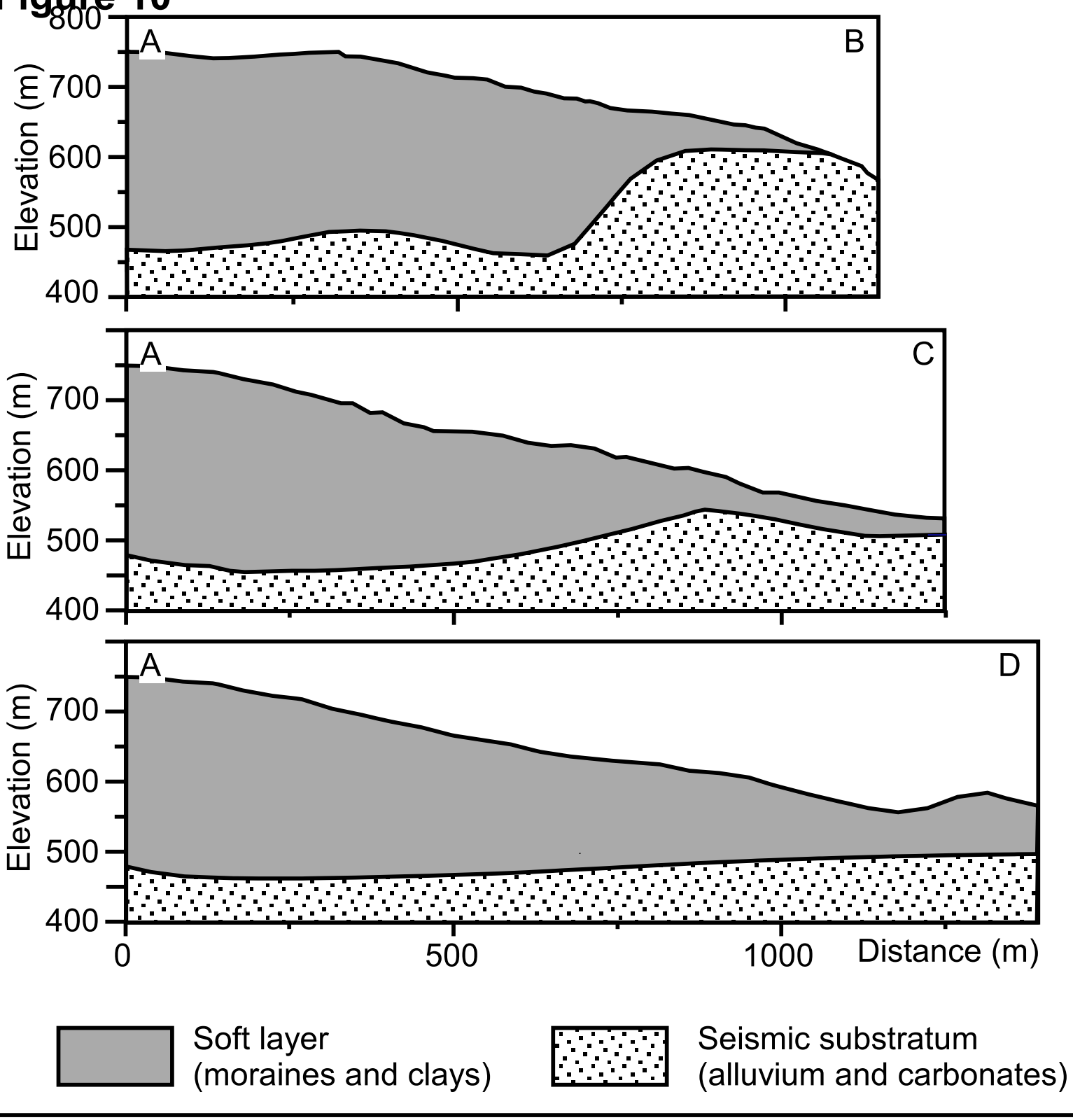
A
B
C
D
Elevation (m)
800
700
600
500
400
0
500
1000
Distance (m)
Soft layer
(moraines and clays)
Seismic substratum
(alluvium and carbonates)